A study on biological roles of GPI-anchor synthesis in the germline development of the nematode Caenorhabditis elegans

村田, 大輔
九州大学大学院システム生命科学府

https://doi.org/10.15017/21716

出版情報：Kyushu University, 2011, 博士（理学）, 課程博士
バージョン：
権利関係：

A study on biological roles of GPI-anchor synthesis in the germline development of the nematode *Caenorhabditis elegans*

村田　大輔

SUMMARY

Glycosylphosphatidylinositol (GPI)-anchor attachment is one of the most common post-translational protein modifications. Using the nematode *Caenorhabditis elegans,* I determined that GPI-anchored proteins are present in germline cells and distal tip cells (DTCs), which are essential for the maintenance of the germline stem cell niche. I identified 24 *C. elegans* genes involved in GPI-anchor synthesis. Inhibition of various steps of GPI-anchor synthesis by RNAi or gene knockout resulted in abnormal development of oocytes and early embryos, and both lethal and sterile phenotypes were observed. The *piga-1* gene (ortholog of human *PIGA*) codes for the catalytic subunit of the phosphatidylinositol N-acetylglucosaminyltransferase complex, which catalyzes the first step of GPI-anchor synthesis. Dr. Shohei Mitani and Dr. Keiko Gengyo-Ando (Tokyo Women's Medical University School of Medicine) isolated *piga-1* knockout worms, and I found that GPI-anchor synthesis is indispensable for the maintenance of mitotic germline cell number. The knockout worms displayed 100% lethality with decreased mitotic germline cells and abnormal eggshell formation. Using cell-specific rescue of the null allele, I showed that expression of *piga-1* in somatic gonads and/or in germline is sufficient for normal embryonic development and the maintenance of the

germline mitotic cells. These results clearly demonstrate that GPI-anchor synthesis is indispensable for germline formation and for normal development of oocytes and eggs.

INTRODUCTION

Glycosylphosphatidylinositol (GPI)-anchors are used by organisms from archaebacteria to humans. Pathogens such as *Trypanosoma cruzi* use GPI-anchor variants to escape from host immune surveillance, and the enzymes involved in their synthesis are potential drug targets for the treatment and prevention of disease (Ikezawa, 2002; Tsukahara *et al.*, 2003).

Paroxysmal nocturnal hemoglobinuria (PNH) is a human acquired genetic disease caused by "somatic" mutation of the X chromosome–linked phosphatidylinositol glycan-class A (*PIGA*) gene in hematopoietic progenitor cells (Nishimura *et al.*, 1999). The *PIGA* gene codes for the major catalytic subunit (subunit A) of the glycosylphosphatidylinositol N-acetylglucosaminyltransferase complex (GPI-GnT; EC 2.4.1.198), which catalyzes the first step of GPI-anchor synthesis. Mutations in this gene would thus inhibit all GPI-anchor synthesis. As a result of the lack of GPI-anchored proteins, the complement system attacks the affected red blood cells, causing hemolysis and hematuria. No heritable form of PNH has been reported, and among the more than 29 genes involved in GPI-anchor synthesis, the only heritable mutations discovered to date in humans are in the *PIGM* promoter region (Almeida *et*

al., 2006; Almeida *et al*., 2009) and in *PIGV* gene, which is deficient in patients with hyperphosphatasia mental retardation (HPMR) syndrome (Mabry syndrome) (Krawitz *et al*., 2010).

One explanation for the rarity of heritable GPI-anchor diseases is that the GPI-modification is not essential, and mutations in these genes result in no adverse phenotypes. The other possibility is that the GPI-anchor modification is so indispensable that most mutations in these genes are lethal, so that organisms with such mutations cannot complete gametogenesis and/or embryonic stages. It is unusual to obtain high chimerism from *Pig-a* (murine *PIGA* ortholog)-disrupted ES cells, and no *Pig-a* knockout mice have been generated, with the exception of a conditional Cre-loxP knockout (Kawagoe *et al*., 1996; Rosti *et al*., 1997; Nozaki *et al*., 1999; Keller *et al*., 1999). Dr. Kazuya Nomura *et al*. previously reported that Ca^{2+}-dependent cell-cell adhesion is mediated by GPI-anchored proteins in *Xenopus laevis* blastula cells. These proteins have partial amino acid sequences identical to that of cortical granule lectin, which is involved in the inhibition of polyspermy during fertilization (Nomura *et al*., 1998).

Based on these results, I planned to study the roles of GPI-anchor synthesis in germline formation and early embryogenesis. Because it is not feasible to observe

gametogenesis and early embryogenesis in ovo in mammals, no information on the roles of GPI-anchors in these fundamental processes has yet been reported. Due to the transparency of its body, I instead used *C. elegans* to study germline cell formation and early embryogenesis. The presence of GPI-anchored proteins in *C. elegans* was first predicted by sequence analysis (Eisenhaber *et al*., 2003), and various GPI-anchor protein predicting algorithms have been developed and used to predict which proteins will be modified by GPI-anchors. For instance, 159 worm proteins are now predicted to be "highly probable" GPI-anchored proteins by the FragAnchor GPI predictor, which is based on the tandem use of a neural network predictor and a hidden Markov model predictor (Poisson *et al*., 2007). By biochemical analysis followed by transfection of protein-coding genes into mammalian cells, several worm proteins (e.g., PHG-1 (Agostoni *et al*., 2002) and WRK-1, see below) have been identified to be GPI-anchored. Recently, Rao *et al*. studied proteins in the membrane raft and showed that two proteins are sensitive to phosphatidylinositol-specific phospholipase C (PI-PLC) treatment, which is frequently used to identify GPI-anchored proteins biochemically (Rao *et al*., 2011). Yet, to our knowledge, no systematic study including histological examination of the proteins has previously been conducted on GPI-anchored proteins in *C. elegans*.

In this study, I examined whether GPI-anchored proteins are present in the *C.*

elegans germline. I found GPI-anchored proteins in oocytes, sperm and other somatic cells of the nematode with fluorescence microscopy and biochemical analysis. I carried out RNAi screening of the worm orthologs of human genes involved in GPI-anchor synthesis and found that inhibition of GPI-anchor synthesis results in germline abnormalities. With *piga-1* knockout worms devoid of GPI-anchor synthesis, I confirmed the essential roles of GPI-anchor synthesis in germline and eggshell formation.

MATERIALS AND METHODS

C. elegans strains

All strains were cultured at 20°C as described previously (Brenner, 1974). N2 Bristol was used as the wild-type strain. The following allele was used in this study: OD70 (*unc-119(ed3)* III;*ltIs44 [P_{pie-1}::mCherry::PH + unc-119(+)]* V) (Kachur *et al.*, 2008). Prior to our experiments, I crossed the OD70 strain with N2 twice. A *piga-1(tm2939)* allele was isolated from pools of worms mutagenized by the TMP/UV method described previously (Gengyo-Ando and Mitani, 2000) with appropriate primers. The *piga-1* deletion mutant was backcrossed 4 times with N2. The *piga-1* mutant was balanced with *mIn1[mIs14 dpy-10(e128)]* II and maintained as a heterozygote (*piga-1(tm2939/+)*) because the homozygous mutant (*piga-1(tm2939)*) was not viable. The *piga-1(tm2939/+)* worm was crossed with the OD70 strain to produce the *piga-1(tm2939/+)*;*ltIs44* worms.

RNAi methodology

All RNAi experiments in this study were performed using the feeding method essentially as described previously (Timmons *et al.*, 2001). *C. elegans* RNAi library

clones (Kamath and Ahringer, 2003) were used for RNAi of most of genes listed in Table 1, except for *Y48E1B.2, T27F7.4, C27A12.9, T22C1.3* and *dpm-1 (Y66H1A.2)*. The cDNA fragments corresponding to these genes except *dpm-1* were amplified from total cDNA of N2 worms by PCR and cloned into the L4440 (pPD129.36) vector. The *dpm-1* genomic sequence was amplified from N2 genomic DNA by PCR and cloned into the L4440 vector. The plasmids were transformed into *E. coli* HT115 (DE3). A single colony of HT115 carrying the plasmids was cultured in LB medium containing 100 μg/ml carbenicillin overnight. The cultured *E. coli* was seeded onto NGM plates and incubated at 37°C overnight. The plates were treated with 2 mM isopropyl-β-D-thiogalactoside (IPTG) and incubated at 37°C for 6 h to allow HT115 to express double-strand RNA. L4 hermaphrodites were transferred onto the feeding plates and maintained at 25°C. I observed the phenotypes of F1 generation after 72 and 96 h. HT115 carrying the L4440 vector without any insert was used as a control. The PCR primers used in this study are listed in Table 7.

Phenotypic analysis

To observe phenotypes of *piga-1 (tm2939)* mutants, L4 larvae of *piga-1(tm2939/+)* and *piga-1(tm2939)* worms were transferred onto separate NGM plates seeded with *E.*

coli OP50 and maintained at 20°C. After 24 h, the animals were observed with a Leica DMRXA full automatic microscope (Leica) (see **Microscopy**).

To count the brood size, L4 larvae were placed onto fresh NGM plates seeded with OP50 (one worm per plate) and maintained at 20°C. The P0 worms were transferred onto fresh NGM plates every 24 h for 3 d. I counted the number of hatched larvae and unhatched eggs on the plates.

Plasmid construction

All plasmids generated in this study were constructed in a pFX_EGFPT vector backbone (Gengyo-Ando *et al*., 2006). For the rescue experiments, I obtained the following promoter sequences for each gene by PCR using N2 genomic DNA as a template: a *lag-2* promoter P_{lag-2} containing 5 kb of upstream sequence and the first codon was specifically expressed in DTCs; a *lim-7* promoter P_{lim-7} containing 3 kb of upstream sequence and the first exon and intron was predominantly expressed in gonadal sheath cells (Voutev *et al*., 2009); a *sth-1* promoter P_{sth-1} containing 1.3 kb of upstream sequence and the first codon was expressed in the spermatheca and uterus (Bando *et al*., 2005). Promoter fragments were inserted into the pFX_EGFPT vector using the TA cloning method described by Ando *et al*. (Gengyo-Ando *et al*., 2006) to

generate P_{lag-2}*::egfp*, P_{lim-7}*::egfp* and P_{sth-1}*::egfp* plasmids. A $P_{eef-1A.2}$*::egfp* plasmid was generated by replacing the *venus* sequence of the $P_{eef-1A.2}$*::venus* vector (Kitagawa *et al*., 2007) with the *egfp* sequence. P_{myo-3}*::egfp*, P_{rgef-1}*::egfp* and $P_{unc-119}$*::egfp* plasmids were generated by Dejima *et al.* (Dejima *et al*., 2010). To generate rescue plasmids expressing the wild-type *piga-1* gene under the control of each promoter, the *piga-1* genomic sequence was amplified from N2 genomic DNA by PCR using appropriate primers tagged with the NotI restriction site. The *piga-1* fragment was digested with NotI and cloned into the NotI restriction site of each plasmid to generate $P_{eef-1A.2}$*::piga-1::egfp*, P_{lag-2}*::piga-1::egfp*, P_{lim-7}*::piga-1::egfp*, P_{sth-1}*::piga-1::egfp*, P_{myo-3}*::piga-1::egfp*, P_{rgef-1}*::piga-1::egfp* and $P_{unc-119}$*::piga-1::egfp*.

For the germline rescue experiment, I constructed the pFX vector containing the promoter, the third intron and the 3' sequence of the *pie-1* gene. First, the 2.4 kb fragment of the *pie-1* promoter was amplified by PCR, and inserted into the pFX_EGFPT vector using the TA cloning method to generate the pFX_P_{pie-1}*::egfp* vector. Second, the third intron sequence (1 kb) of the *pie-1* gene was amplified by PCR, and inserted into the BamHI site located upstream the *pie-1* promoter sequence of the pFX_P_{pie-1}*::egfp* vector. This addition of the third intron to the upstream of the *pie-1* promoter enhances gene expression (Strome *et al*., 2001). Third, the *pie-1* 3’ sequence

(1.4 kb) was amplified by PCR and inserted into the BglII/PciI sites located downstream the *egfp* coding sequence of the pFX_$P_{pie\text{-}1}$*::egfp* vector. Finally, the *piga-1* genomic sequence was inserted into the NotI site located between the *pie-1* promoter and the *egfp* coding sequence to generate the $P_{pie\text{-}1}$*::piga-1::egfp* plasmid.

For expression analysis of *wrk-1,* the coding sequence was amplified from N2 genomic DNA by PCR using appropriate primers tagged with the NotI and BglII restriction sites. The *wrk-1* fragment was digested with NotI and BglII and cloned into the NotI- and BglII- double digested pFX vector (pFX_*wrk-1* vector). To insert the coding sequence of EGFP into the pFX_*wrk-1* vector, the coding sequence of EGFP was amplified from the pFX_EGFPT vector by PCR using appropriate primers tagged with the BamHI restriction site. The *egfp* fragment was digested with BamHI and inserted into the BamHI restriction site of the *wrk-1* sequence (pFX_*egfp-tagged wrk-1* vector, see Figure 1, D and E). Five kilobases of the *wrk-1* promoter were amplified by PCR using primers tagged with the NotI restriction site. The *wrk-1* promoter fragment was digested with NotI and inserted into the NotI restriction site of the pFX_*egfp-tagged wrk-1* vector to generate the $P_{wrk\text{-}1}$*::egfp-tagged wrk-1* plasmid. DNA sequence analysis was performed with a 3130 Genetic Analyzer (Applied Biosystems). The PCR primers used in this study are listed in Table 7.

Microinjection

Microinjections were performed as described by Mello and Fire (Mello and Fire, 1995). For expression analysis of the *egfp-tagged wrk-1*, the $P_{wrk\text{-}1}$*::egfp-tagged wrk-1* plasmid was injected at 15-20 ng/μl with a coinjection marker pRF4 *(rol-6(su1006))* at 80 ng/μl into the gonads of adult N2 and the *piga-1(tm2939/+)*hermaphrodites.

For rescue experiments of the *piga-1(tm2939)*, the rescue plasmids were injected into the gonads of the adult *piga-1(tm2939/+)* hermaphrodites. The $P_{eef\text{-}1A.2}$*::piga-1::egfp* plasmid was injected at 5 ng/μl with pRF4 at 100 ng/μl. The $P_{lag\text{-}2}$*::piga-1::egfp*, $P_{myo\text{-}3}$*::piga-1::egfp* and $P_{rgef\text{-}1}$*::piga-1::egfp* plasmids were injected at 10 ng/μl with pRF4 at 90 ng/μl. The $P_{lim\text{-}7}$*::piga-1::egfp*, $P_{sth\text{-}1}$*::piga-1::egfp* and $P_{unc\text{-}119}$*::piga-1::egfp* plasmids were injected at 20 ng/μl with pRF4 at 80 ng/μl.

For the germline rescue experiment, microinjections were performed as previously described (Kelly *et al.*, 1997). For the generation of complex extrachromosomal arrays, DNAs were digested and linearized with restriction enzymes, and then the digested DNAs were injected into the gonads of the adult *piga-1(tm2939/+)* hermaphrodites. The rescue plasmid (*pFX_*$P_{pie\text{-}1}$*::piga-1::egfp*), pRF4 and N2 genomic DNA were digested with PvuII, EcoRI and XbaI, respectively. XbaI fragments the *piga-1* gene in the N2

genomic DNA. The PvuII-digested *pFX_P$_{pie-1}$::piga-1::egfp* was injected at 0.5 ng/μl with EcoRI-digested pRF4 at 0.5 ng/μl and XbaI-digested N2 genomic DNA fragment at 31 ng/μl. To circumvent germline silencing of the transgenes, injected animals were maintained at 25°C. Transgenic worms were selected and maintained based on their EGFP expression and roller phenotype.

Selection of the *piga-1 (tm2939)* rescue lines

I injected the rescue plasmid into the gonads of *piga-1(tm2939/+)* hermaphrodites to obtain *piga-1(tm2939/+)* transgenic lines (see **Microinjection**). To examine whether the introduced transgene could rescue the *piga-1(tm2939)* mutants, ten *piga-1(tm2939)* mutants expressing the transgene were transferred onto a fresh NGM plate seeded with OP50 and cultured at 20°C except for the germline rescue experiment at 25°C. After several days, I determined whether the mutants with the transgene could produce offspring on the plate. Homozygous mutant lines that carried the transgene and were capable of fertility were counted as rescue lines. Three independent experiments were performed for each line.

FLAER staining

Alexa-488 proaerolysin (FLAER) was obtained from Protox Biotech (Canada). For FLAER staining, gonads were dissected and covered with an 18 × 18 mm coverslip. The gonads were then freeze-cracked and fixed in methanol at –20°C for 10 min. They were immediately transferred to PBS to prevent drying. The slides were washed twice in fresh PBS for 5 min and blocked with 1% bovine serum albumin (BSA) in PBS for 30 min at room temperature in a humid chamber. FLAER diluted in PBS (final concentration of 20-50 nM) was applied, and the specimens were incubated for 2 h at room temperature in a dark humid chamber. After incubation, the slides were washed twice in PBS for 5 min and stained with 4, 6-diamidino-2-phenylindole (DAPI) diluted in PBS (final concentration of 5 μg/ml) for 10 min. Slides were then washed twice in PBS for 10 min and mounted in VECTASHIELD Mounting Medium (Vector Laboratories).

Immunofluorescent staining

Adult hermaphrodites 24 h after L4 stage were used for immunofluorescent staining. Gonads were dissected and covered with an 18 × 18 mm coverslip. The gonads were freeze-cracked and fixed in methanol at –20°C for 5 min and then immediately transferred to PBS. The slides were washed twice in fresh PBS for 5 min and once in

PBS containing 0.05% Tween 20 (PBST) for 5 min. Slides were blocked with 1% BSA/PBST for 30 min at room temperature in a humid chamber. Specimens were incubated with primary antibody diluted 1:1,000 in 1% BSA/PBST at 4°C overnight in a humid chamber. The following primary antibodies were used: rabbit polyclonal IgG anti-phospho-histone H3 (Ser10) antibody (MILLIPORE) and mouse monoclonal IgG anti-GFP antibody mFX73 (Wako). The slides were then washed twice in PBS and incubated with secondary antibody diluted 1:200 in PBS at room temperature for 2 h in a dark humid chamber. The secondary antibodies were as follows: Alexa Fluor 594 goat anti-rabbit IgG and Alexa Fluor 594 goat anti-mouse IgG (Molecular Probes). After incubation, the slides were washed twice in PBS for 5 min and stained with DAPI (final concentration of 5 μg/ml in PBS) for 10 min. Finally, the slides were washed twice in PBS for 10 min and mounted in VECTASHIELD Mounting Medium (Vector Laboratories).

Eggshell permeability assay

For eggshell permeability assay, embryos were dissected in egg buffer (118 mM NaCl, 48 mM KCl, 2 mM $CaCl_2$, 2 mM $MgCl_2$, 25 mM HEPES, pH 7.3) containing 8 μM FM4-64 (Molecular Probes). The osmolality of egg buffer (340 mOsm) was

measured with OSMOMAT 030-D Osmometer (Gonotec GmbH, Germany).

Microscopy

Differential interference contrast (DIC) and fluorescent images were obtained with a Leica DMRXA full automatic microscope (Leica). The acquired images were processed using MetaMorph software (version 6.1r5, Universal Imaging). Confocal images were acquired with a LSM 510 META (Carl Zeiss). Worms were placed on an 8-well printed microscope slide glass (Matsunami Glass) and were anesthetized with M9 buffer containing 16 mM sodium azide.

Precondensation of Triton X-114

Precondensation of Triton X-114 (Sigma) was performed according to the previously described method (Hooper, 1992). In preparation**,** 50 ml of Tris-buffered saline (TBS, 10 mM Tris-HCl, 150 mM NaCl, pH 7.4) was mixed with 0.8 mg of butylated hydroxytoluene. This solution was gently mixed with 1 ml of Triton X-114 and placed on ice for 3 h. The solution was incubated at 30°C overnight to induce condensation of Triton X-114. After the incubation, the upper phase (aqueous phase) was removed. The remaining lower phase (detergent-rich phase) was mixed with an

equal volume of fresh TBS and placed on ice for 3 h. The condensation procedure was then repeated twice. The resulting detergent-rich phase was used as a precondensed Triton X-114.

Fractionation of GPI-anchored proteins

Fractionation of GPI-anchored proteins was performed according to the previously described method (Hooper, 1992). The lyophilized fraction of total proteins was dissolved in Tris-buffered saline (TBS) containing 2 mM EDTA and 1 mM PMSF. The solution was gently mixed with precondensed Triton X-114 on ice and incubated at 4°C overnight. The sample was centrifuged at 15,000 × g at 4°C for 20 min to remove detergent-insoluble materials. The supernatant was then incubated at 37°C for 10 min and centrifuged at 13,000 × g for 5 min at room temperature to induce Triton X-114 phase partition. The upper phase (aqueous phase) was removed, and the lower phase (detergent-rich phase) was gently mixed with fresh TBS on ice. The phase partition method was repeated twice more. The resulting detergent-rich phase was mixed with 4 volumes of ice-cold acetone and incubated at –20°C overnight to remove the detergent and concentrate proteins. The sample was centrifuged at 13,000 × g for 30 min at 4°C. The supernatant was removed and the precipitate was dried to evaporate remaining

acetone. The precipitate was then dissolved in 200 μl of Tris-HCl buffer (10 mM Tris-HCl, pH 7.4) and gently mixed with 1 μl of phosphatidylinositol-specific phospholipase C (PI-PLC, Molecular Probes) on ice. After incubation at 37°C for 90 min, the sample was gently mixed with 200 μl of TBS and 60 μl of precondensed Triton X-114 on ice. After the phase partition procedure, the upper phase (aqueous phase) was recovered and mixed with fresh precondensed Triton X-114 on ice. This phase partition was then repeated. The upper phase underwent acetone precipitation at –20°C overnight as described above. After centrifugation at 13,000 × g for 30 min at 4°C, the supernatant was removed. The resulting precipitate was dissolved in fresh TBS, and this solution was used as a GPI-anchored protein-enriched fraction.

Identification of proteins by LC/MS/MS

The extracted GPI-anchored proteins were separated by SDS-PAGE and stained with SYPRO Ruby (Molecular Probes) or with Silver Stain MS kit (WAKO, Japan) according to the manufacturers' protocols. Noticeable bands were cut into pieces and incubated in 30 mM DTT at 56°C for 1 h. The gel pieces were subsequently incubated in 69 mM sodium iodoacetate at 28°C for 45 min in the dark and then divided into two tubes. To one tube was added sequence grade-modified trypsin (wt:wt 1:50; Promega) in

25 mM ammonium bicarbonate, and the mixture was incubated at 37°C for 16 h. After the reaction was quenched by acidification with 1% trifluoroacetic acid (Wako), the digest was subjected to SpeedVac concentration (Thermo Fisher Scientific) and reconstituted in 0.1% formic acid.

The peptides were separated in a C18 column (Magic C18 0.2 × 150 mm, 3 μ; Michrom Bioresources) at a flow rate of 3 μl/min in an HPLC system (Paradigm MS4; Michrom Bioresources). The eluents were 2% acetonitrile/0.1% formic acid (pump A) and 90% acetonitrile/0.1% formic acid (pump B). The peptides were eluted with a linear gradient of 5-65% in pump B for 20 min and analyzed using an on-line linear ion trap mass spectrometer (Finnigan LTQ; Thermo Fisher Scientific) with a single mass scan (m/z 450-2,000) and a data-dependent MS/MS scan in the positive ion mode. All product ions were submitted to the computer database search analysis with the Mascot search engine (Matrixscience) and TurboSEQUEST search engine (Thermo Fisher Scientific) using the NCBI database (*C. elegans*).

Statistical analysis

Statistical analyses, including one-way ANOVA followed by Holm's multiple comparison test, were performed using R statistical package (R version 2.11.0).

RESULTS

Identification of GPI-anchored proteins in *C. elegans*

To determine whether GPI-anchors are present in *C. elegans*, I initially performed fluorochrome (Alexa 488)-labeled inactivated aerolysin (FLAER) staining. FLAER is an *Aeromonas hydrophila* toxin that binds specifically to GPI-anchored proteins (Brodsky *et al*., 2000; Hong *et al*., 2002). Cell membranes of oocytes and sperm in the dissected gonad were brightly stained by FLAER (Figure 1A), as were distal tip cells (DTCs) and their processes (Figure 1B). Similar bright fluorescence was detected in cell membranes of muscles and neurons in adult hermaphrodites (data not shown). These results strongly suggest that GPI-anchors are present in germline cells and somatic cells of the nematode. Next, I fractionated total proteins from wild-type N2 worms to identify GPI-anchored proteins. Potential GPI-anchored proteins were isolated by phase partition with the detergent Triton X-114 (Hooper, 1992; Nomura *et al*., 1998). In this method, membrane proteins and GPI-anchored proteins are partitioned into the detergent-rich phase, whereas soluble proteins remain in the aqueous phase. The proteins in the detergent-rich phase were treated with PI-PLC to specifically cleave GPI-anchors, and the Triton X-114 phase partitioning was repeated. The proteins that moved to the

aqueous phase after PI-PLC treatment were analyzed by SDS-PAGE (Figure 1C). Twelve protein bands were cut out of the gel, and the protein sequences were identified using mass spectrometry (LC/MS/MS). Forty-two proteins were identified, and their sequences were scanned for possible GPI-anchor modification signal sequences using the Big-PI (Eisenhaber *et al.*, 2003), GPI-SOM (Fankhauser and Maser, 2005), FragAnchor (Poisson *et al.*, 2007) and PredGPI (Pierleoni *et al.*, 2008) programs. Twenty-two proteins were predicted to be GPI-anchored by at least two different programs (Table 1).

One of the GPI-anchor candidate proteins identified was WRK-1. WRK-1 is an ortholog of the *Drosophila* Wrapper protein, which belongs to the immunoglobulin superfamily and is GPI-anchored (Boulin *et al.*, 2006). The behavior of the WRK-1 protein was examined *in vivo* by transgenic analysis with EGFP-tagged WRK-1 protein (Figure 1, D-F). The tagged protein was detected in the cell membranes of DTCs and muscle cells, and disruption of GPI-anchor synthesis resulted in abnormal accumulation of the protein inside DTCs (Figure 6D). These results demonstrate that WRK-1 is GPI-anchored and that the Triton X-114 phase partitioning reliably separated GPI-anchored proteins. Thus, *C. elegans* has GPI-anchored proteins that are widely expressed in oocytes, sperm, DTCs, muscle, neurons and other cell types.

Knockdown of genes involved in *C. elegans* GPI-anchor synthesis

After confirming the presence of GPI-anchored proteins in the nematode, I next asked whether genes involved in GPI-anchor synthesis are conserved between nematodes and humans. More than 29 different genes are involved in human GPI-anchor synthesis (Kinoshita *et al*., 2007). Through a PSI-BLAST search using human gene sequences, I confirmed the presence of 24 orthologous genes in the *C. elegans* genome, although no orthologs for *PIGH*, *PIGY*, *PIGL*, *PIGF* or *DPM2* were identified (Figure 2 and Table 2). Knockdown phenotypes of these genes were analyzed by feeding RNAi. Suppression of GPI-anchor synthesis resulted in abnormalities in oogenesis, fertilization, and embryogenesis (Figure 3 and Table 2). Single RNAi against the following orthologous genes resulted in the sterile progeny phenotype, where no oocytes or eggs were present in adult F1 hermaphrodites (*C. elegans* sequence names in parentheses): *PIGP* (*Y48E1B.2*), *PIGV* (*T09B4.1*), *PIGO* (*C27A12.9*), *PIGK* (*T05E11.6*), *PIGU* (*T22C1.3*), *GAA1* (*F33D11.9*), *MPDU1* (*F38E1.9*), and *DPM3* (*F28D1.11*).

To visualize membrane abnormalities in germline cells, I used the OD70 strain ($P_{pie\text{-}1}$*::mCherry::PH (PLC delta1)*) for RNAi analysis. PIGP is one of the subunits of the GPI-GnT complex that catalyzes the first step of GPI-anchor synthesis, in which

PIGA is the catalytic subunit. *PIGP* (*Y48E1B.2*) RNAi yielded F1 adult animals without fertilized or unfertilized eggs (32%, *n*=576, Figure 3A). In the affected F1 animals, oocyte formation was also defective, and the gonads contained no matured oocytes (Figure 3C, 71%, *n*=24). In some animals, although oocytes were formed, they were irregular in shape (Figure 3D, 29%, *n*=24). In the single RNAi knockdowns of the *PIGV*, *PIGO*, and GPI transamidase orthologs (subunit genes *PIGK*, *PIGU*, and *GAA1*), oocytes just past the spermatheca showed no indication of cleavage, and abnormally dislocated mCherry membrane materials were detected in the cytosol and around the nuclei of oocytes (Figure 3E). Severe defects were observed in eggshell formation. In oocytes just past the spermatheca, no eggshells were visible, and fertilization seemed to be defective. PIGV and PIGO transfer the second mannose and third mannose, respectively to the glycosylphosphatidylinositol during GPI precursor assembly. The GPI transamidase (PIGK, PIGU, and GAA1) mediates GPI anchoring in the endoplasmic reticulum by replacing a protein's C-terminal GPI attachment signal peptide with a pre-assembled GPI. Thus, RNAi inhibition of the first step of GPI-anchor synthesis (*PIGP*), of the attachment of mannoses to GPI (*PIGV* and *PIGO*), and of the attachment of the GPI-anchor to proteins (*PIGK*, *PIGU*, and *GAA1*) resulted in severe defects in oogenesis. No morphological, growth or movement abnormalities were

observed in the F1 worms. These results indicate that GPI-anchor synthesis is essential for normal development of germline cells, oocytes and eggs in *C. elegans*.

Isolation and analysis of *piga-1* knockout allele *tm2939*

Among the 24 orthologous genes involved in GPI-anchor synthesis, *DPM1*, *DPM3* and *MPDU1* (*SL15*) are involved in the synthesis of the sugar donor dolichol phosphate-mannose, which is required in the synthesis of N-linked/O-linked oligosaccharides and for the synthesis of GPI-anchors (Figure 2 and Table 2). Thus, the RNAi phenotypes of each gene including larval arrest, scrawny larvae and germline defects could have resulted from N-/O-glycosylation inhibition as well as GPI-anchor inhibition (see Table 2 and Figure 4). To distinguish phenotypes solely derived from GPI-anchor synthesis from N-/O-glycosylation defects, it is important to choose genes that are not involved in N-/O-glycosylation for further study. For this reason, I chose the *C. elegans* gene *piga-1* (ortholog of human *PIGA*), which is conserved among eukaryotes. In humans, the GPI-GnT enzyme complex consists of seven subunits: PIGA, PIGC, PIGH, PIGP, PIGQ, PIGY, and DPM2. There is only one *PIGA* ortholog (*piga-1*: *D2085.6*) in the worm genome (on chromosome II), whose predicted amino acid sequence and catalytic site are well conserved among various species (human PIGA and

worm PIGA-1 are 52.3% identical and 76.7% similar; Figure 5). Because I observed no abnormalities in embryos treated with *piga-1* RNAi, Dr. Shohei Mitani and Dr. Keiko Gengyo-Ando (Tokyo Women's Medical University School of Medicine) isolated a deletion allele of the *piga-1* gene by screening the TMP/UV-induced deletion library with appropriate primers. The deletion allele (*tm2939*) lacked 324 bp of the *piga-1* sequence, including exon 3 and exon 4 (Figure 6A). The deletion introduced a frameshift mutation and should produce a null allele. Homozygous embryos (*piga-1(tm2939)*) born from heterozygotes (*piga-1(tm2939/+)*) grew to the adult stage, but the worms moved slowly and had a scrawny phenotype (Figure 6B). The body length of the *piga-1(tm2939)* adult hermaphrodites was reduced. Homozygous adult worms laid no eggs and many lethal eggs were observed in the uterus. The lethal eggs included cleavage-arrested embryos at various stages, from “before first-cleavage” embryos to multicellular embryos (Figure 6E). The lethality of the F1 eggs was 100% (n > 100). No FLAER staining was observed in the gonads of *piga-1(tm2939)* worms, strongly indicating that GPI-anchor synthesis was totally inhibited (Figure 6C). To confirm that the synthesis of GPI-anchored proteins is inhibited in *piga-1* knockout worms, I generated a transgenic *tm2939* line expressing EGFP-tagged WRK-1 by transgene microinjection. On the *piga-1* null background, membrane sorting of WRK-1

in the DTCs was inhibited, and WRK-1 was not present on the cell surface but was instead retained inside the cell (compare Figure 6D with Figure 1F). Thus, GPI-anchor attachment was inhibited in the *piga-1* deficient worms.

To gain insights into the nature of the lethality of the affected eggs, I examined whether the eggs from the *piga-1* null allele showed changes in osmotic sensitivity (Kaitna *et al.*, 2002). In two-thirds of the eggs dissected from *piga-1* null animals, the shape of the eggshell was abnormal (n=144), suggesting defects in the eggshells (Figure 7C-F). The integrity of the eggshell barrier to small molecules was examined with the lipophilic dye FM4-64 (Sato *et al.*, 2008) which stains membrane structures. The eggshell of a wild-type embryo is composed of a vitelline layer, a chitinous middle layer and a lipid-rich inner layer (Rappleye *et al.*, 1999). FM4-64 cannot normally pass through the mature eggshell, preventing staining of the cells within the eggshell. Conversely, embryos with a defective eggshell inner layer do stain with FM4-64 (Rappleye *et al.*, 1999; Johnston *et al.*, 2006). When I stained dissected eggs with FM4-64 dye, the wild-type eggshells were not permeable to the dye, and only eggshells and polar bodies were stained (Figure 7G and Table 3). In 25% of the *piga-1(tm2939)* embryos, the eggshells were permeable, and the dye stained blastomere membranes. This indicates that loss of GPI-anchor synthesis results in changes in eggshell

permeability. Under the standard osmolarity supported condition (340 mOsm egg buffer; Strange *et al.*, 2007), I still observed abnormalities of egg development (Figure 8), indicating the abnormal phenotypes are not merely resulted from osmotic abnormality.

In addition to the osmotic phenotypes, abnormalities of gonads and intestine were detected in the null worms. The length of the gonadal arms was decreased, and in some animals, the morphology of the gonad was distorted, with wrinkled gonadal arms (Figure 9A). The width of the intestine and the number of intestinal granules also decreased (Figure 9B). Thus, the *piga-1* deletion mutant worm *tm2939* is deficient in GPI-anchored proteins in the cell membrane and shows severe germline abnormalities, including embryonic lethality, as well as various somatic abnormalities.

Somatic or germline expression of *piga-1* rescues abnormal phenotypes of the null worms

To confirm that these phenotypes were due to deletion of *piga-1*, I injected the wild-type *piga-1* gene (*D2085.6* genomic sequence) driven by the *eef-1A.2* promoter ($P_{eef\text{-}1A.2}$*::piga-1::egfp*) into *tm2939* worms. The *eef-1A.2* gene (*eft-4*) codes for translational elongation factor 1α, and its promoter drives its expression in almost all

cell types. The wild-type *piga-1* gene driven with this promoter rescued all of the germline and embryonic defects observed in the *tm2939* homozygous animals (Table 4 and Figure 10A). The EGFP fluorescence of the transgene products indicated that the PIGA-1 protein was expressed in somatic cells, and the lack of EGFP fluorescence and EGFP immunoreactivity in the germline indicated that PIGA-1 expression was suppressed in the germline (Figure 10A). The germline expression of transgenes is silenced by a germline silencing mechanism (Green *et al*., 2008). Thus, I was not sure whether PIGA-1 expression in the germline rescued the abnormal phenotypes. To circumvent the germline silencing of the *piga-1* gene, I next injected the wild-type *piga-1* gene driven by *pie-1* promoter with cut DNA to rescue the *piga-1* null allele (Kelly *et al.*, 1997). The worms were cultured at 25℃ to suppress germline silencing. As shown in Figure 7G, Figure 10D and in Table 4, all abnormalities of the null allele, including eggshell permeability defects were rescued by expressing the wild-type *piga-1* gene in the germline. The PIGA-1 fluorescence was solely detected in the germline, and no EGFP-tagged PIGA-1 was detected in somatic cells (Figure 10D). The embryonic lethality of the null allele was almost completely rescued (Figure 10F). From these two rescue experiments, I conclude that synthesis of GPI-anchored proteins either in the somatic cells or in the germline is sufficient for the development of germline cells and

normal embryogenesis.

Expression of *piga-1* in somatic gonad is sufficient to rescue the null allele

Although the wild-type *piga-1* gene driven by the *eef-1A.2* promoter rescued all of the abnormalities in germline formation and embryogenesis, germline expression of the gene seemed to be suppressed by germline silencing. Thus, in this rescue experiment, the *piga-1* gene expressed in somatic tissues might have been responsible for the complete rescue of the GPI-anchor–deficient phenotypes in germline cells and embryos. To identify somatic tissue and cells responsible for this successful rescue of the null allele, I generated a wild-type *piga-1*::*egfp* gene linked to several different tissue-specific promoters, and microinjected them to rescue the *tm2939* strain (Table 4). To our surprise, *piga-1* driven by the DTC-specific promoter $P_{lag\text{-}2}$ rescued the germline phenotypes most effectively. The osmotic permeability phenotype was also rescued completely (Figure 7G and Table 3). *lag-2* expression from this promoter in adult gonad is limited to the DTCs and excluded from the germline (Henderson *et al.*, 1994), and the *lag-2* promoter specifically drives the expression of the introduced transgenes in DTCs. I examined the presence of EGFP fluorescence as well as immunoreactive EGFP protein in the rescued animals by fluorescence microscopy and by immunostaining with

anti-GFP antibody. Only DTCs were positive for PIGA-1 (Figure 10B and Figure 11A left column). Neither the EGFP signal nor EGFP-tagged protein was observed in the germline of the rescued worms. Thus, there was little possibility of the expression of the wild-type *piga-1* transgene in the germline, and I concluded that the transgene P_{lag-2}*::piga-1::egfp* was expressed only in DTCs. In contrast, the *piga-1* transgene expressed in the spermatheca and the uterus (P_{sth-1}*::piga-1::egfp*) did not rescue the phenotypes (Table 4). The muscle-specific promoter (P_{myo-3}) and the pan-neuronal promoter (P_{rgef-1}) were also unable to rescue the defects. $P_{unc-119}$, another pan-neuronal promoter, successfully rescued the phenotype, but I detected weak GFP expression in DTCs as well as in neuronal cells (data not shown), confirming the importance of *piga-1* expression in DTCs. The expression of the transgene in gonadal sheath cells (P_{lim-7}*::piga-1::egfp*) provided weak rescue activity (Figure 10C and Table 4). These rescued worms grew slowly (Figure 12), and brood size recovery was poor (Figure 10E). Furthermore, the embryonic lethality of this rescue line was higher than that of other three rescue lines (Figure 10F).

In mammalian cells, intercellular transfer of GPI-anchored proteins occurs (Dunn *et al*., 1996). Thus, I examined whether GPI-anchored proteins synthesized in DTCs could be transferred to the germline of the transgenically rescued worms. As shown in Figure

13, I detected weak but positive FLAER staining on the oocyte cell surface of the $P_{lag\text{-}2}$*::piga-1::egfp* rescued worms. The FLAER signal in mitotic germline cells was too weak to detect, and only oocyte signals were detected in the experiment. The presence of GPI-anchored proteins was detected in oocytes but not in sperm (Figure 13). Because the *piga-1* gene is active in DTCs and DTCs extend processes proximally, the GPI-anchored proteins synthesized in the DTCs could be transferred to the germline mitotic cells by direct contact or transferred by extensive secretion, which is characteristic of DTCs (Hall *et al*., 1999). The results show that the expression of the *piga-1* gene in DTCs accompanied by the transfer of GPI-anchored proteins to the germline was sufficient for the complete rescue of the germline defects.

Loss of GPI-anchor synthesis affects germline mitotic cell number

DTCs express the Notch ligand LAG-2, which maintains germline stem cells at the distal end of gonadal arms in the undifferentiated state. DTCs are linked to oocyte precursor mitotic cells (including germline stem cells) and provide the LAG-2 signal. DTCs therefore have been thought to form the germline stem cell niche (Byrd and Kimble, 2009; Cinquin *et al.*, 2010). Decreasing the LAG-2 signal induces germline stem cells to switch from mitosis to meiosis, resulting in oocyte maturation. As shown

in Figure 1B, GPI-anchored proteins are present on DTCs. In addition, our data demonstrate that germline cell formation was severely affected by the loss of genes involved in GPI-anchor synthesis. To examine the effects of *piga-1* deficiency on mitotic germline cells, the mitotic cells in dissected gonads were labeled by immunostaining with anti-phosphohistone H3 (anti-pH3) antibody, which is a marker of mitosis (Hendzel *et al.*, 1997). The number of mitotic prometaphase nuclei (pH3-positive) was significantly reduced in *piga-1(tm2939)* worms (Figure 14, A and B). The average number of pH3-positive cells of the *piga-1(tm2939)* worm was 0.6±0.9 (n=13) compared with 3.7±2.2 (n=18) in the wild-type worm. Induction of DTC-specific expression of the *piga-1* gene led the prometaphase nucleus number to recover to normal levels. The average number of pH3-positive cells in the rescued mutant ($P_{lag\text{-}2}$*::piga-1* worm) was 3.2±2.3 (n=17). Expression of *piga-1* from the *eef-1A.2* promoter also restored the pH3-positive cell number to the normal level, while the *lim-7* promoter was less effective. When *piga-1* was expressed in the germline from the *pie-1* promoter, the number of pH3-positive cells returned to the normal level (Figure 14C). These results indicate that PIGA-1 synthesis in somatic gonad and/or germline cells is sufficient to restore the number of prometaphase mitotic cells to the normal level, showing the importance of GPI-anchored proteins in germline mitotic cell

number maintenance. From these results, I conclude that GPI-anchor synthesis in the germline and/or DTCs (somatic gonad) is sufficient for maintaining normal numbers of mitotic germline cells.

DISCUSSION

Here, I demonstrated that GPI-anchor synthesis in the somatic gonad and/or in the germline is indispensable in the germline formation and embryonic development of the nematode *C. elegans*. Abnormal germline phenotypes of the GPI-anchor–deficient worm were successfully rescued by expressing wild-type *piga-1* (ortholog of human *PIGA*) in the somatic gonad (DTCs or gonadal sheath cells) or in the germline. Total inhibition of GPI-anchor synthesis by *piga-1* knockout resulted in severe germline malformation beginning at the distal end of the gonad, as well as eggshell malformation at the proximal end of the gonad.

GPI-anchored proteins are embedded in the outer leaflet of the plasma membrane, and they are generally more highly concentrated at the membrane rafts than transmembrane proteins. This high concentration seems to be essential for signal transduction (Yamashita and Fukushima, 2007; Lingwood and Simons, 2010). In the present experiments, the recruitment of proteins to the cell membrane by GPI-anchor modification was blocked as shown in Figure 6D. Thus, inhibition of GPI-anchor synthesis could affect various signal transduction pathways that are important in germline formation, and the total lack of GPI-anchored proteins on the cell surface

seems to be the major cause of the germline and eggshell abnormalities described in this study. Synthesis of GPI-anchored proteins seems to be essential for reproduction of this species.

Our transgenic rescue experiment using wild-type *piga-1::egfp* driven by the *lag-2* promoter demonstrates that expression of PIGA-1 in DTCs is sufficient for the total rescue of the germline phenotypes. Because no PIGA-1 was detected in the germline cells, the FLAER staining of proximal oocytes strongly indicated that the GPI-anchored proteins in the oocytes originated from DTCs. The transfer of GPI-anchored proteins from DTCs to the germline is highly probable while the possibility that non-detectable amounts of PIGA-1 are present in the germline and in other somatic cells cannot be excluded altogether. It is possible that the GPI-anchor moiety from one protein is recycled and attached to another protein. Thus, the GPI-anchored proteins found in oocytes are not necessarily identical to the GPI-anchored proteins in DTCs. As shown in Figure 13, oocytes were stained with FLAER, but sperm were not stained at all. The sperm are separated from other germline cells by the spermatheca, and they are situated at the most proximal position of the gonad. The physical separation of sperm from DTCs may be the reason for the loss of FLAER staining in these cells. At present, I have no evidence that GPI-anchored proteins are normally transferred from the DTCs to

the germline in wild type worms, and I cannot exclude the possibility that this transfer is an emergency response of the somatic gonad to the lack of PIGA-1 synthesis in the germline. Further experiments are needed to resolve this question.

Recently, GPI-anchor modification has been used to deliver GPI-linked therapeutic proteins to target cells with a transcellular transfer mechanism. GPI-anchored therapeutic proteins added from outside of the cells are incorporated into lipid rafts, after which they leave the rafts and move to cytoplasmic lipid droplets. The lipid droplets can be secreted as exosomes or microvesicles, and incorporated into the membranes of nearby cells (Müller, 2010). In the present study, the transgenic expression of *piga-1* in DTCs rescued all of the germline phenotypes of the *piga-1* null worms. The results strongly indicate that intercellular transfer of GPI-anchored proteins from DTCs to germline cells rescued the germline phenotypes completely, and the transfer seems to be very efficient. Our results suggest the intriguing possibility that intercellular transport of GPI-anchored proteins could be used to deliver drugs to nearby tissues and cells. The transgenically rescued worm described in this paper could be used as a model system to examine the utility of drug delivery systems based on GPI-anchor modification.

Proteome analyses of the transgenically rescued worms and wild-type N2 worms

were carried out to determine what kinds of GPI-anchored proteins are synthesized in these worms and which proteins are important for germline and eggshell development (Figure 15, Table 5 and 6). GPI-anchored proteins were identified with Triton X-114 phase partitioning followed by PI-PLC digestion. The isolated proteins were separated by SDS-PAGE, silver-stained and analyzed by LC/MS/MS. Table 5 and 6 show all of the GPI-anchored proteins predicted by the PredGPI and FragAnchor programs that Dr. Kazuko H. Nomura and I identified in three different experiments. Most of the proteins listed in Table 1 were also identified in these experiments, and many new candidate GPI-anchored proteins were identified.

In *Drosophila melanogaster*, male hub cells and female cap cells play similar roles to nematode DTCs in forming the *Drosophila* germline stem cell niche (Fuller *et al*., 2007). Dally is a GPI-anchored heparan sulfate proteoglycan of the glypican family in *Drosophila*. Dally is expressed in the female cap cells, and another glypican, Dally-like, is expressed in the male hub cells. Dally and Dally-like are required for maintaining the germline stem cell niches in female and male *Drosophila*, respectively (Guo *et al*., 2009; Hayashi *et al*., 2009). *C. elegans* has two members of the glypican family, LON-2 and GPN-1. I did not detect either protein in our proteome analyses. The knockout/knockdown phenotypes and the expression patterns of these worm glypican

genes are different from the germline phenotypes described in this paper, indicating different roles of these genes in development (Foehr *et al*., 2006; Hudson *et al*., 2006; Gumienny *et al*., 2007). *C. elegans* glypicans may not be involved in the maintenance of the germline stem cell niche.

The Notch signaling pathway plays important roles in germline stem cell niche formation at the distal end of the gonad of the nematode. Because inhibition of GPI-anchor synthesis resulted in decreased mitotic cell number at the distal end of the gonad, I suspect the involvement of GPI-anchored proteins in Notch signaling. In the present proteome analyses, however, canonical Notch ligands such as LAG-2 and ten other DSL ligands (*apx-1*, *arg-2*, *lag-2*, and *dsl-1* to *dsl-7*) were not detected in the GPI-anchored protein fraction. Both PredGPI and FragAnchor predict that these ligands are not GPI-anchored. An examination of the identified GPI-anchored protein candidates in the Table 6 shows that Jagged-like GPI-anchored protein (C02B10.3) was present in the GPI-anchored protein fraction from *lag-2* promoter–rescued worms. This protein has sequence homology to human tanascins, Jagged-1, Notch2, and Notch3. Although the GPI-anchored protein RIG-6, which is a non-canonical Notch ligand and a homolog of contactin, was not detected in the present proteome analysis, RNAi against *rig-6* affected germline development (our unpublished result). Therefore, the

involvement of the non-canonical Notch signaling pathway in germline development is an intriguing possibility for future studies.

The possible GPI-anchored proteins identified in this study include the neuronal IgCAM homologue RIG-3, an integrin β subunit, cathepsin A homologue Y40D12A.2, growth–arrest specific protein homologue PHG-1 (PHAS-1), Ephrin-B2 homologue VAB-2, and WRK-1. WRK-1 is the prototypical GPI-anchored protein expressed in the DTCs. The deletion mutant alleles of *wrk-1* (*tm1099* and *ok695*) show neuronal but not germline abnormalities (Boulin *et al.*, 2006). This implies that WRK-1 may not be the GPI-anchored protein required for normal germline development. WRK-1 interacts with an ephrin (VAB-2) and an ephrin receptor (VAB-1). VAB-2/EFN-1 is a predicted GPI-anchored ephrin ligand for VAB-1, and RNAi against *vab-1* results in embryonic lethality (Partridge *et al.*, 2008). VAB-2/EFN-1 is predominantly expressed in neurons, but Serial Analysis of Gene Expression (SAGE) analysis shows that the gene is also expressed in the germline (Wang *et al.*, 2009). VAB-2 was detected in our proteome analysis of *lag-2* promoter–rescued worms. These results suggest that the VAB-2 expressed in germline cells or DTCs is one of the GPI-anchored proteins responsible for the germline phenotypes described in this study. No single gene knockdown results in the aforementioned germline phenotypes (Wormbase 220). One plausible explanation

for this is that there is no single GPI-anchored protein species responsible for the phenotypes, but the synthesis of several different GPI-anchored proteins is necessary for the normal development of the germline and eggshells. Based on the results presented in this paper, I am planning to carry out multiple knockouts/knockdowns of these GPI-anchored proteins and to examine the expression timing and localization of these GPI-anchored molecules. Genetic analysis and reverse-genetic analysis will also play important roles in resolving the molecular mechanisms of the functions of GPI-anchored proteins in germline and egg development.

REFERENCES

Agostoni, E., Gobessi, S., Petrini, E., Monte, M., and Schneider, C. (2002). Cloning and characterization of the *C. elegans gas1* homolog: *phas-1*. Biochim Biophys Acta *1574*, 1-9.

Almeida, A. M. *et al.* (2006). Hypomorphic promoter mutation in *PIGM* causes inherited glycosylphosphatidylinositol deficiency. Nat. Med. *12*, 846-851.

Almeida, A., Layton, M., and Karadimitris, A. (2009). Inherited glycosylphosphatidyl inositol deficiency: a treatable CDG. Biochim. Biophys. Acta *1792*, 874-880.

Bando, T., Ikeda, T., and Kagawa, H. (2005). The homeoproteins MAB-18 and CEH-14 insulate the dauer collagen gene *col-43* from activation by the adjacent promoter of the spermatheca gene *sth-1* in *Caenorhabditis elegans*. J. Mol. Biol. *348*, 101-112.

Boulin, T., Pocock, R., and Hobert, O. (2006). A novel Eph receptor-interacting IgSF protein provides *C. elegans* motoneurons with midline guidepost function. Curr. Biol.

16, 1871-1883.

Brenner, S. (1974). The genetics of *Caenorhabditis elegans*. Genetics *77*, 71-94.

Brodsky, R. A., Mukhina, G. L., Li, S., Nelson, K. L., Chiurazzi, P. L., Buckley, J. T., and Borowitz, M. J. (2000). Improved detection and characterization of paroxysmal nocturnal hemoglobinuria using fluorescent aerolysin. Am. J. Clin. Pathol. *114*, 459-466.

Byrd, D. T., and Kimble, J. (2009). Scratching the niche that controls *Caenorhabditis elegans* germline stem cells. Semin. Cell Dev. Biol. *20,* 1107-1113.

Cinquin, O., Crittenden, S. L., Morgan, D. E., and Kimble, J. (2010). Progression from a stem cell-like state to early differentiation in the *C. elegans* germ line. Proc. Natl. Acad. Sci. USA *107*, 2048-2053.

Dejima, K. *et al.* (2010). Two Golgi-resident 3'-phosphoadenosine 5'-phosphosulfate transporters play distinct roles in heparan sulfate modifications and embryonic and

larval development in *Caenorhabditis elegans*. J. Biol. Chem. *285*, 24717-24728.

Dunn, D. E., Yu, J., Nagarajan, S., Devetten, M., Weichold, F. F., Medof, M. E., Young, N. S., and Liu, J. M. (1996). A knock-out model of paroxysmal nocturnal hemoglobinuria: Pig-a(-) hematopoiesis is reconstituted following intercellular transfer of GPI-anchored proteins. Proc. Natl. Acad. Sci. USA *93*, 7938-7943.

Eisenhaber, F., Eisenhaber, B., Kubina, W., Maurer-Stroh, S., Neuberger, G., Schneider, G., and Wildpaner, M. (2003). Prediction of lipid posttranslational modifications and localization signals from protein sequences, big-Pi, NMT and PTS1. Nucleic Acids Res. *31*, 3631-3634.

Fankhauser, N., and Maser, P. (2005). Identification of GPI anchor attachment signals by a Kohonen self-organizing map. Bioinformatics *21*, 1846-1852.

Foehr, M. L., Lindy, A. S., Fairbank, R. C., Amin, N. M., Xu, M., Yanowitz, J., Fire, A. Z., and Liu, J. (2006). An antagonistic role for the *C. elegans* Schnurri homolog SMA-9 in modulating TGFβ signaling during mesodermal patterning. Development *133*,

2887-2896.

Fuller, M. T., and Spradling, A. C. (2007). Male and female *Drosophila* germline stem cells: Two versions of immortality. Science *316*, 402-404.

Gengyo-Ando, K., and Mitani, S. (2000). Characterization of mutations induced by ethyl methanesulfonate, UV, and trimethylpsoralen in the nematode *Caenorhabditis elegans*. Biochem. Biophys. Res. Commun. *269*, 64-69.

Gengyo-Ando, K., Yoshina, S., Inoue, H., and Mitani, S. (2006). An efficient transgenic system by TA cloning vectors and RNAi for *C. elegans*. Biochem. Biophys. Res. Commun. *349*, 1345-1350.

Green, R. A., Audhya, A., Pozniakovsky, A., Dammermann, A., Pemble, H., Monen, J., Portier, N., Hyman, A., Desai, A., and Oegema, K. (2008). Expression and imaging of fluorescent proteins in the *C. elegans* gonad and early embryo. Methods Cell. Biol. *85*, 179-218.

Gumienny, T. L., MacNeil, L. T., Wang, H., de Bono, M., Wrana, J. L., and Padgett, R. W. (2007). Glypican LON-2 is a conserved negative regulator of BMP-like signaling in *Caenorhabditis elegans*. Curr. Biol. *17*, 159-164.

Guo, Z., and Wang, Z. (2009). The glypican Dally is required in the niche for the maintenance of germline stem cells and short-range BMP signaling in the *Drosophila* ovary. Development *136*, 3627-3635.

Hall, D. H., Winfrey, V. P., Blaeuer, G., Hoffman, L. H., Furuta, T., Rose, K. L., Hobert, O., and Greenstein, D. (1999). Ultrastructural features of the adult hermaphrodite gonad of *Caenorhabditis elegans*: relations between the germ line and soma. Dev. Biol. *212*, 101-123.

Hayashi, Y., Kobayashi, S., and Nakato, H. (2009). *Drosophila* glypicans regulate the germline stem cell niche. J. Cell Biol. *187*, 473-480.

Henderson, S. T., Gao, D., Lambie, E. J., and Kimble, J. (1994). *lag-2* may encode a signaling ligand for the GLP-1 and LIN-12 receptors of *C. elegans*. Development *120*,

2913-2924.

Hendzel, M.J., Wei, Y., Mancini, M. A., Van Hooser, A., Ranalli, T., Brinkley, B. R., Bazett-Jones, D. P., and Allis, C. D. (1997). Mitosis-specific phosphorylation of histone H3 initiates primarily within pericentromeric heterochromatin during G2 and spreads in an ordered fashion coincident with mitotic chromosome condensation. Chromosoma *106*, 348-360.

Hong, Y., Ohishi, K., Inoue, N., Kang, J. Y., Shime, H., Horiguchi, Y., van der Goot, F. G., Sugimoto, N., and Kinoshita, T. (2002). Requirement of N-glycan on GPI-anchored proteins for efficient binding of aerolysin but not *Clostridium septicum* α-toxin. EMBO J. *21*, 5047-5056.

Hooper, N. M. (1992). Identification of a glycosylphosphatidylinositol anchor on membrane proteins. In: Lipid modification of proteins: a practical approach, ed. Hooper, N.M. and Turner, A.J., Oxford, IRL PRESS, 89-115.

Hudson, M. L., Kinnunen, T., Cinar, H. N., and Chisholm, A. D. (2006). *C. elegans*

Kallmann syndrome protein KAL-1 interacts with syndecan and glypican to regulate neuronal cell migrations. Dev. Biol. *294*, 352-365.

Ikezawa, H. (2002). Glycosylphosphatidylinositol (GPI)-anchored proteins. Biol. Pharm. Bull. *25*, 409-417.

Johnston, W. L., Krizus, A., and Dennis, J. W. (2006). The eggshell is required for meiotic fidelity, polar-body extrusion and polarization of the *C. elegans* embryo. BMC Biol. *4*, 35.

Kachur, T. M., Audhya, A., and Pilgrim, D. B. (2008). UNC-45 is required for NMY-2 contractile function in early embryonic polarity establishment and germline cellularization in *C. elegans*. Dev. Biol. *314*, 287-299.

Kaitna, S., Schnabel, H., Schnabel, R., Hyman, A. A., and Glotzer, M. (2002). A ubiquitin C-terminal hydrolase is required to maintain osmotic balance and execute actin dependent processes in the early *C. elegans* embryo. J. Cell Sci. *115*, 2293-2302.

Kamath, R. S., and Ahringer, J. (2003). Genome-wide RNAi screening in *Caenorhabditis elegans*. Methods *30*, 313-321.

Kawagoe, K., Kitamura, D., Okabe, M., Taniuchi, I., Ikawa, M., Watanabe, T., Kinoshita, T., and Takeda, J. (1996). Glycosylphosphatidylinositol-anchor-deficient mice: implications for clonal dominance of mutant cells in paroxysmal nocturnal hemoglobinuria. Blood *87*, 3600-3606.

Keller, P., Tremml, G., Rosti, V., and Bessler, M. (1999). X inactivation and somatic cell selection rescue female mice carrying a *Piga*-null mutation. Proc. Natl. Acad. Sci. USA *96*, 7479-7483.

Kelly, W. G., Xu, S., Montgomery, M. K., and Fire, A. (1997). Distinct requirements for somatic and germline expression of a generally expressed *Caenorhabditis elegans* gene. Genetics *146*, 227-238.

Kinoshita, T., Murakami, Y. and Morita, Y. S. (2007). Diseases associated with GPI anchors. In: Comprehensive Glycoscience, ed. Kamerling, J.P. *et al.*, Amsterdam,

Elsevier Ltd., vol. 4, Chap 4.21, pp393-419.

Kitagawa, H. *et al.* (2007). Expression of *rib-1*, a *Caenorhabditis elegans* homolog of the human tumor suppressor EXT genes, is indispensable for heparan sulfate synthesis and embryonic morphogenesis. J. Biol. Chem. *282*, 8533-8544.

Krawitz, P. M. *et al*. (2010). Identity-by-descent filtering of exome sequence data identifies PIGV mutations in hyperphosphatasia mental retardation syndrome. Nat. Gen. *42*, 827-829.

Lingwood, D., and Simons, K. (2010). Lipid rafts as a membrane-organizing principle. Science *327*, 46-50

Mello, C., and Fire, A. (1995). DNA transformation. Methods Cell Biol. *48*, 451-482.

Müller, G. (2010). Oral delivery of protein drugs: Driver for personalized medicine?. Curr. Issues Mol. Biol. *13*, 13-24.

Nishimura, J., Murakami, Y., and Kinoshita, T. (1999). Paroxysmal nocturnal hemoglobinuria: An acquired genetic disease. Am. J. Hematol. *62*, 175-182.

Nomura, K. H., Kobayashi, R., Hirabayashi, Y., Fujisue-Sakai, M., Mizuguchi, S., and Nomura, K. (1998). Involvement of blood-group-B-active trisaccharides in Ca^{2+}-dependent cell-cell adhesion in the *Xenopus* blastula. Dev. Genes Evol. *208*, 9-18.

Nozaki, M., Ohishi, K., Yamada, N., Kinoshita, T., Nagy, A., and Takeda, J. (1999). Developmental abnormalities of glycosylphosphatidylinositol-anchor-deficient embryos revealed by Cre/loxP system. Lab. Invest. *79*, 293-299.

Partridge, F.A., Tearle, A.W., Gravato-Nobre, M.J., Schafer, W.R., Hodgkin, J. (2008). The *C. elegans* glycosyltransferase BUS-8 has two distinct and essential roles in epidermal morphogenesis. Dev. Biol. *317*, 549-559.

Pierleoni, A., Martelli, P. L., and Casadio, R. (2008). PredGPI: a GPI-anchor predictor. BMC Bioinformatics *9*, 392.

Poisson, G., Chauve, C., Chen, X., and Bergeron, A. (2007). FragAnchor: a large-scale predictor of glycosylphosphatidylinositol anchors in eukaryote protein sequences by qualitative scoring. Genomics Proteomics Bioinformatics *5*, 121-130.

Rao, W., Isaac, R. E., and Keen, J. N. (2011). An analysis of the *Caenorhabditis elegans* lipid raft proteome using geLC-MS/MS. J. Proteomics *74*, 242-253.

Rappleye, C. A., Paredez, A. R., Smith, C. W., McDonald, K. L., and Aroian, R. V. (1999). The coronin-like protein POD-1 is required for anterior-posterior axis formation and cellular architecture in the nematode *Caenorhabditis elegans*. Genes Dev. 13, 2838-2851.

Rosti, V., Tremml, G., Soares, V., Pandolfi, P. P., Luzzatto, L., and Bessler, M. (1997). Murine embryonic stem cells without *pig-a* gene activity are competent for hematopoiesis with the PNH phenotype but not for clonal expansion. J. Clin. Invest. *100,* 1028-1036.

Sato, M., Grant, B. D., Harada, A., and Sato, K. (2008). Rab11 is required for

synchronous secretion of chondroitin proteoglycans after fertilization in *Caenorhabditis elegans*. J. Cell Sci. *121*, 3177-3186.

Strange, K., Christensen, M., and Morrison, R. (2007). Primary culture of *Caenorhabditis elegans* developing embryo cells for electrophysiological, cell biological and molecular studies. Nat Protoc. *2*, 1003-1012.

Strome, S., Powers, J., Dunn, M., Reese, K., Malone, C. J., White, J., Seydoux, G., and Saxton, W. (2001). Spindle dynamics and the role of γ-tubulin in early *Caenorhabditis elegans* embryos. Mol. Biol. Cell *12*, 1751-1764.

Timmons, L., Court, D. L., and Fire, A. (2001). Ingestion of bacterially expressed dsRNAs can produce specific and potent genetic interference in *Caenorhabditis elegans*. Gene *263*, 103-112.

Tsukahara, K. *et al*. (2003). Medicinal genetics approach towards identifying the molecular target of a novel inhibitor of fungal cell wall assembly. Mol. Microbiol. *48*, 1029-1042.

Voutev, R., Keating, R., Hubbard, E. J. A., and Vallier, L. G. (2009). Characterization of the *Caenorhabditis elegans* Islet LIM-homeodomain ortholog, *lim-7*. FEBS Letters *583*, 456-464.

Wang, X., Zhao, Y., Wong, K., Ehlers, P., Kohara, Y., Jones S. J., Marra, M. A., Holt, R. A., Moerman, D. G, and Hansen, D. (2009). Identification of genes expressed in the hermaphrodite germ line of *C. elegans* using SAGE. BMC Genomics. *10*:213.

Yamashita, K., and Fukushima, K. (2007). Carbohydrate recognition by cytokines and its relevance to their physiological activities. In: Comprehensive Glycoscience, ed. Kamerling, J.P. *et al.* , Amsterdam, Elsevier Ltd., vol. 3, Chap. 3.25, pp539-562.

ACKNOWLEDGMENTS

First, I thank Dr. Kazuya Nomura for his support in my doctoral course, and Dr. Kazuko H. Nomura, Dr. Katsufumi Dejima and Dr. Souhei Mizuguchi for their experimental support. I also thank Prof. Shohei Mitani and Dr. Keiko Gengyo-Ando (Tokyo Women's Medical University School of Medicine) for isolating and providing the mutant worm strain, Prof. Katsuko Yamashita and Dr. Keiko Fukushima (Tokyo Institute of Technology, Yokohama) for critical comments on my study, and Dr. Nana Kawasaki, Dr. Satsuki Ito, Ms. Yukari Nakajima (National Institute of Health Sciences, Tokyo), Dr. Masaki Matsumoto from the Division of Proteomics of the Medical Institute of Bioregulation (Kyushu University), Mizuho Oda and Emiko Koba from the Laboratory for Technical Support of the Medical Institute of Bioregulation (Kyushu University) for the LC/MS/MS analysis. I acknowledge the *Caenorhabditis Genetics Center* for the strains used in this study, which is funded by the NIH National Center for Research Resources (NCRR). This work was supported by the Core Research for Evolutional Science and Technology Program of the Japan Science and Technology Corp. to K. N. This work was also supported partially by Grant-in-Aid for JSPS Fellows (to K. D.), Grant-in-Aid for Young Scientists (B) (to S. M.), and Grant-in-Aid for

Challenging Exploratory Research (to K. N.) from MEXT, Japan.

Figure 1

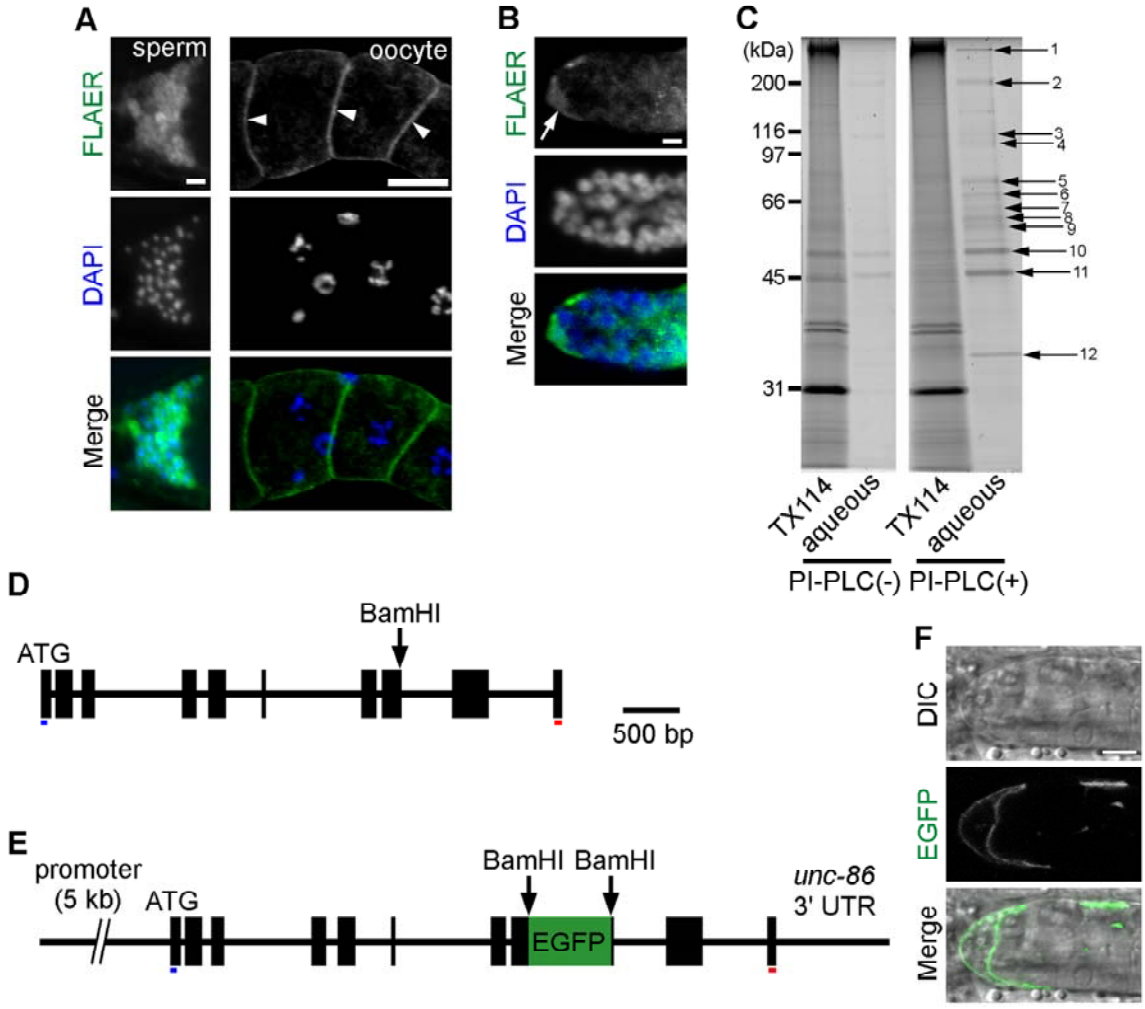

Figure 1. GPI-anchored proteins in wild-type *C. elegans* germline.
(A) Dissected gonadal arm stained with Alexa 488-labeled proaerolysin (FLAER, green). Oocytes (arrowheads) and sperm were strongly labelled by FLAER. Bars, 5 μm (left column) and 20 μm (right column).
(B) Distal tip cell (DTC) expressing GPI-anchored proteins. Strong FLAER staining is observed in DTC (arrow) with its cytonemes. Bar, 5 μm.
(C) GPI-anchored proteins concentrated by Triton X-114 (TX114) phase partitioning followed by phosphatidylinositol-specific phospholipase C (PI-PLC) treatment were analyzed by SDS-PAGE. SDS-PAGE of the detergent-rich phase (TX114) and aqueous phase are shown before (PI-PLC (-)) and after PI-PLC treatment (PI-PLC (+)). Numbered arrows indicate possible GPI-anchored proteins.
(D) Structure of the *wrk-1 (F41D9.3)* gene isoform b (*wrk-1b*). Black boxes indicate exons.
(E) Schematic of an *egfp-tagged wrk-1b* reporter gene construct. The coding sequence of EGFP was inserted into the BamHI restriction site in exon 8 of the *wrk-1b* gene. Blue and red underlines indicate the predicted coding sequences of the N-terminal signal sequence and the C-terminal GPI-anchor modification signal, respectively.
(F) A typical GPI-anchored protein, WRK-1, in DTCs. EGFP-tagged WRK-1 proteins are visible on the DTC surface. Bar, 5 μm.

Figure 2

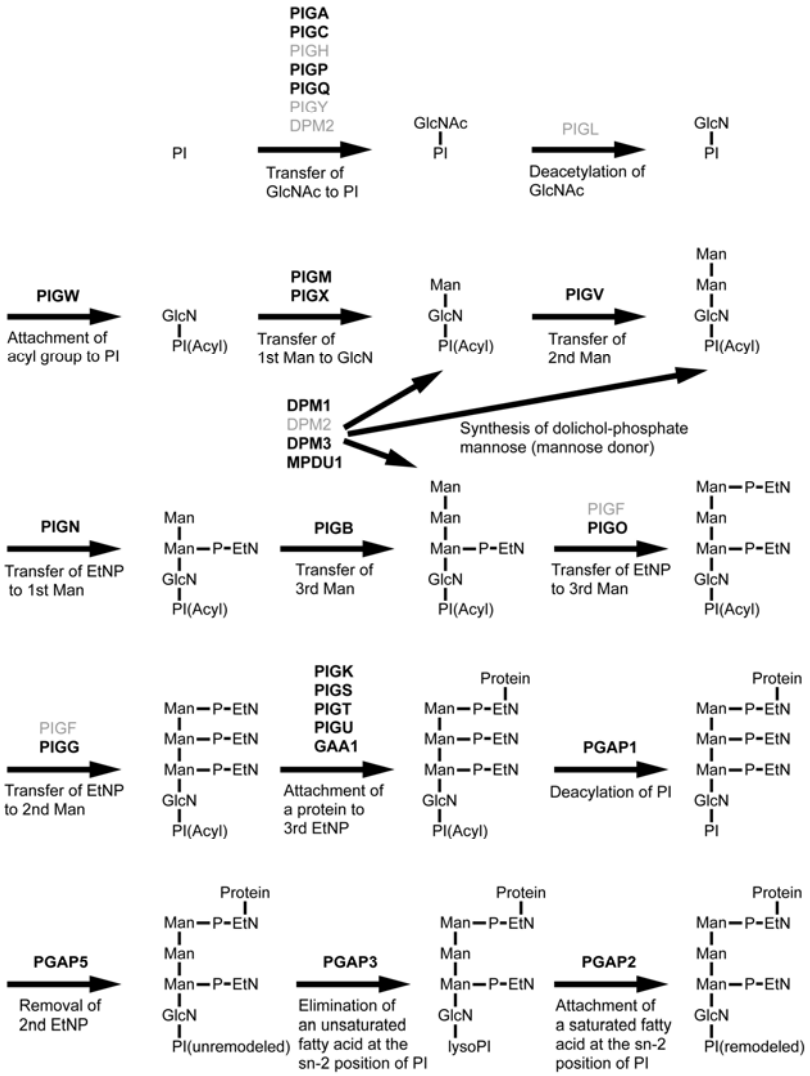

Figure 2. GPI-anchor synthesis in the mammalian cells.
The orthologous genes found in the *C. elegans* genome are shown in bold black text (See Table 2). PI, phosphatidylinositol; GlcNAc, N-acetylglucosamine; GlcN, glucosamine; Man, mannose; P-EtN, ethanolamine phosphate.

Figure 3

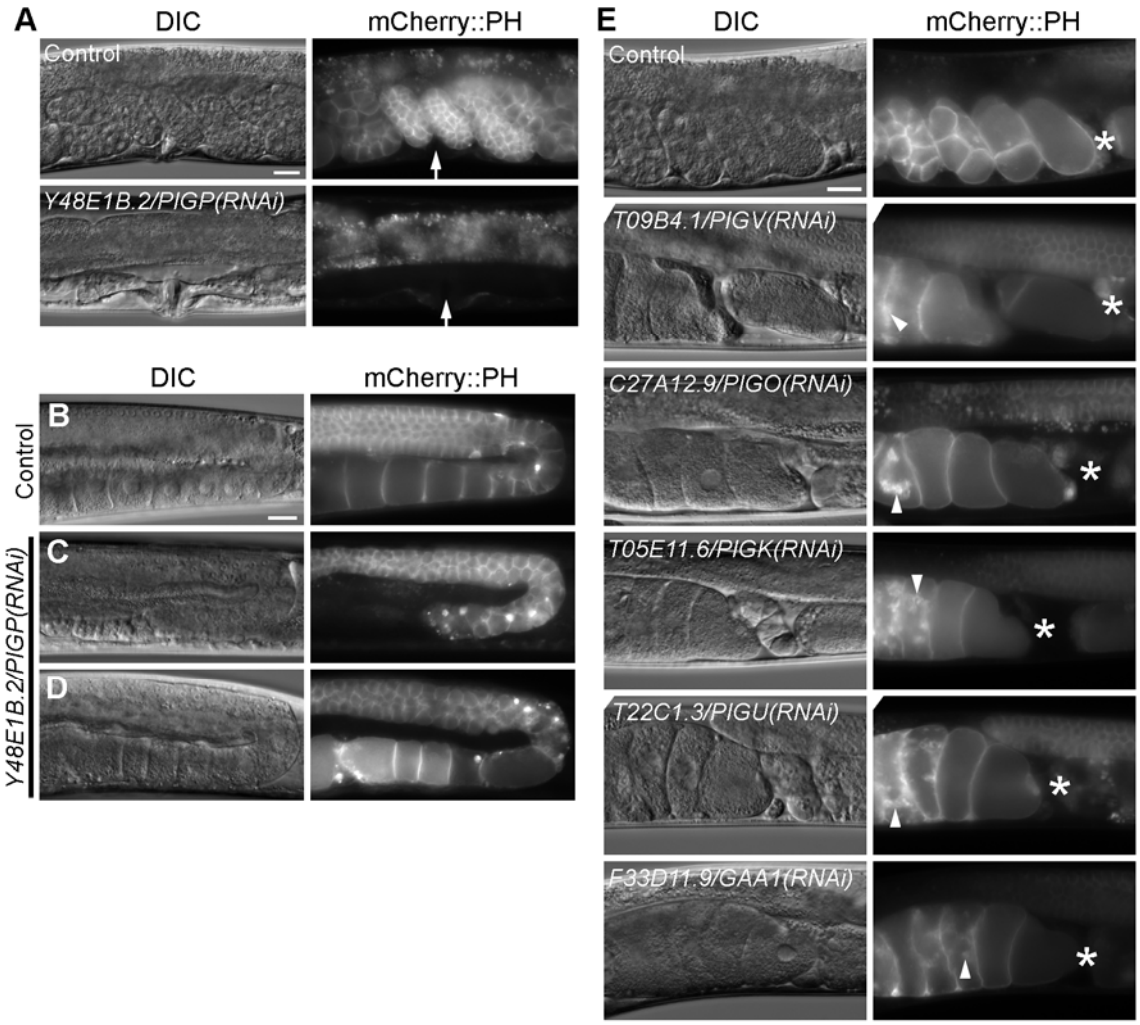

Figure 3. RNAi mediated knockdown of genes involved in GPI-anchor synthesis results in severe germline phenotypes.
(A) In typical *Y48E1B.2*/*PIGP* RNAi-treated worms, no eggs were found in the uteri. Arrows indicate the position of the vulva.
(B-D) Abnormalities of germline cells in *Y48E1B.2*/*PIGP* RNAi-treated worms with no eggs (A). Wild-type gonad with normal oocytes in control RNAi-treated worms (B). Gonad without matured oocytes (C) and with irregularly shaped oocytes (D) in *Y48E1B.2/PIGP* RNAi–treated worms.
(E) Knockdown of *T09B4.1/PIGV*, *C27A12.9/PIGO,* and the GPI transamidase complex (*T05E11.6/PIGK*, *T22C1.3/PIGU*, and *F33D11.9/GAA1*) resulted in abnormal oocytes just past the spermatheca. Dislocated membrane materials labelled with mCherry::PH were observed around the nuclei and in the cytosol of abnormal oocytes in the uteri (arrowheads). Asterisks indicate the spermatheca.
Bars, 20 μm.

Figure 4

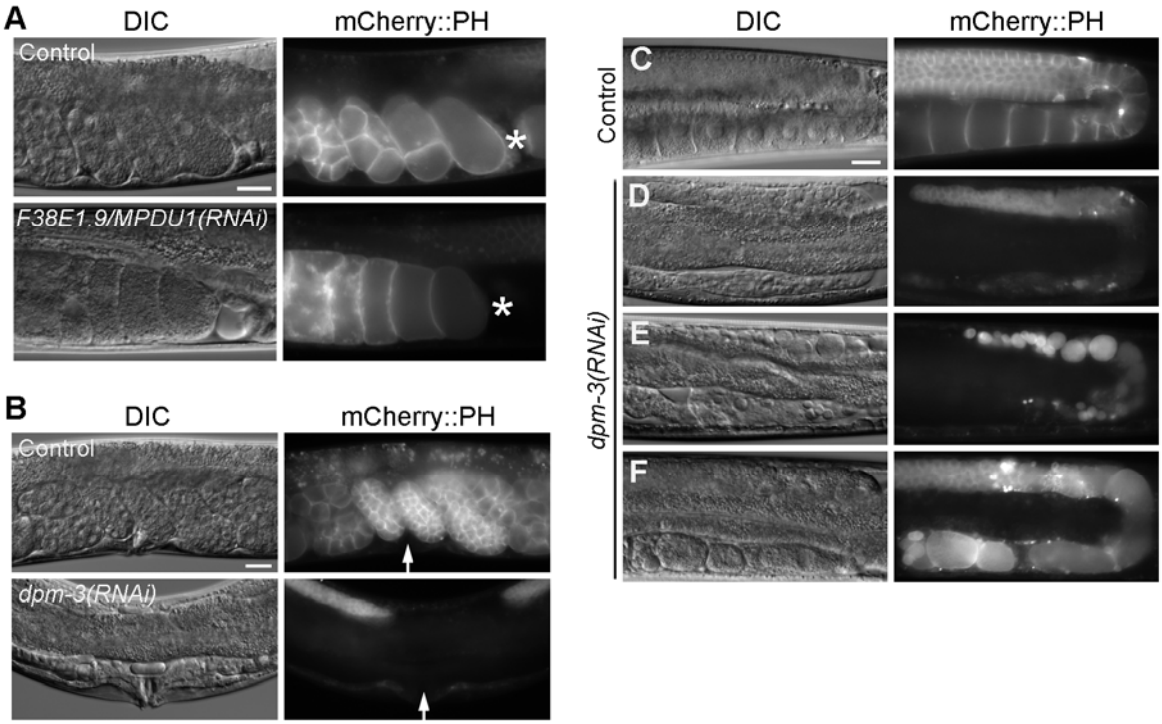

Figure 4. RNAi of genes involved in the synthesis of both GPI-anchor and N-linked/O-linked oligosaccharides resulted in severe germline phenotypes.

(A) Knockdown of the *F38E1.9/MPDU1* resulted in the oocyte abnormality similar to the phenotype shown in Figure 3E. Asterisks indicate the spermatheca.

(B) In *dpm-3* RNAi-treated worms, no eggs were found in the uteri. Arrows indicate the position of the vulva.

(C-F) Abnormalities of germline cells in *dpm-3* RNAi-treated worms with no eggs (B). Wild-type gonad with normal oocytes in control RNAi-treated worms (C). Gonad with no matured oocytes (D, 42%, *n*=24), with disrupted germ cell proliferation and germline syncytium (E, 33%, *n*=24) and with irregularly shaped oocytes (F, 25%, *n*=24) in *dpm-3* RNAi-treated worms.

Bars, 20 μm.

Figure 5

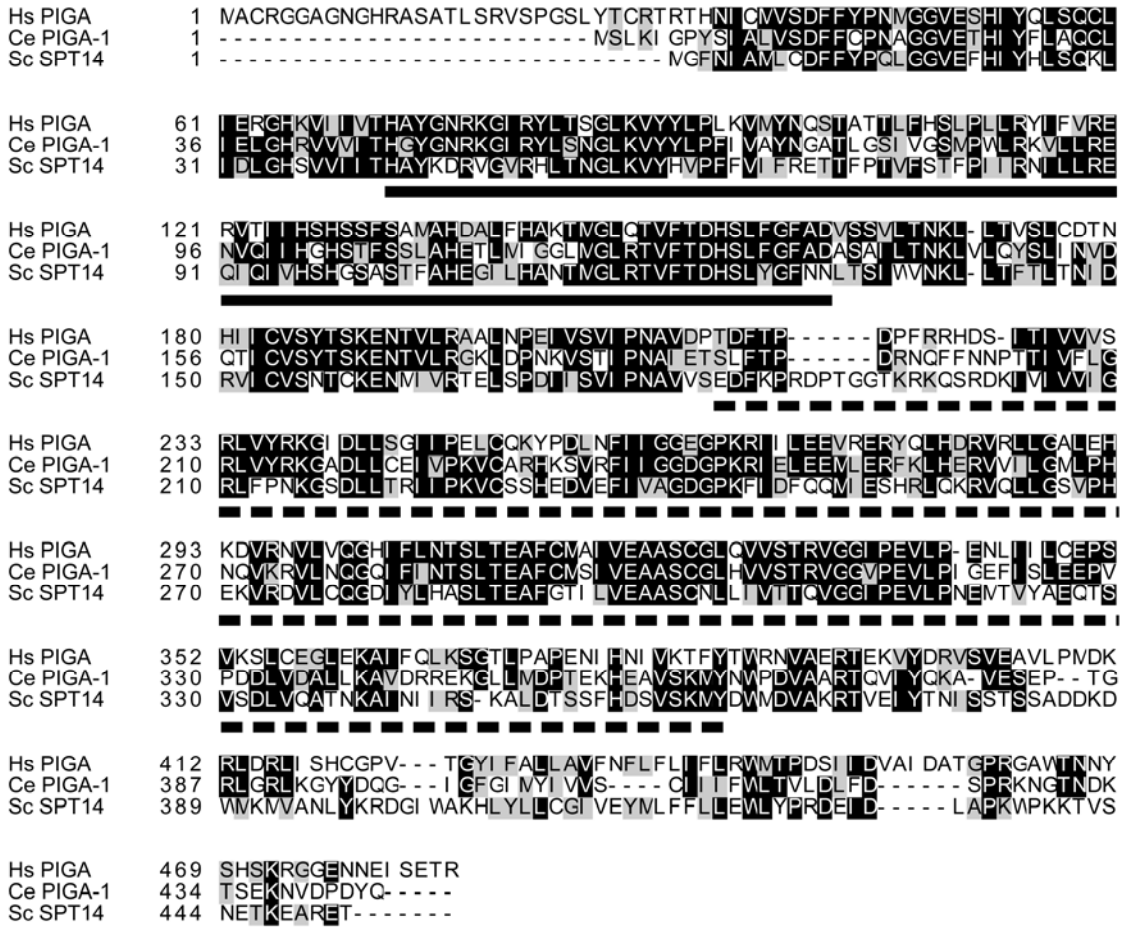

Figure 5. ClustalW alignment of the predicted amino acid sequences of *H. sapiens* PIGA (Hs PIGA), *C. elegans* PIGA-1 (Ce PIGA-1) and *S. cerevisiae* SPT14 (Sc SPT14).

Identical amino acids are shaded in black and similar amino acids are shaded in gray. The PIGA domain is underlined with a solid line, and the glycosyltransferase group 1 domain is shown as a dashed line.

Figure 6

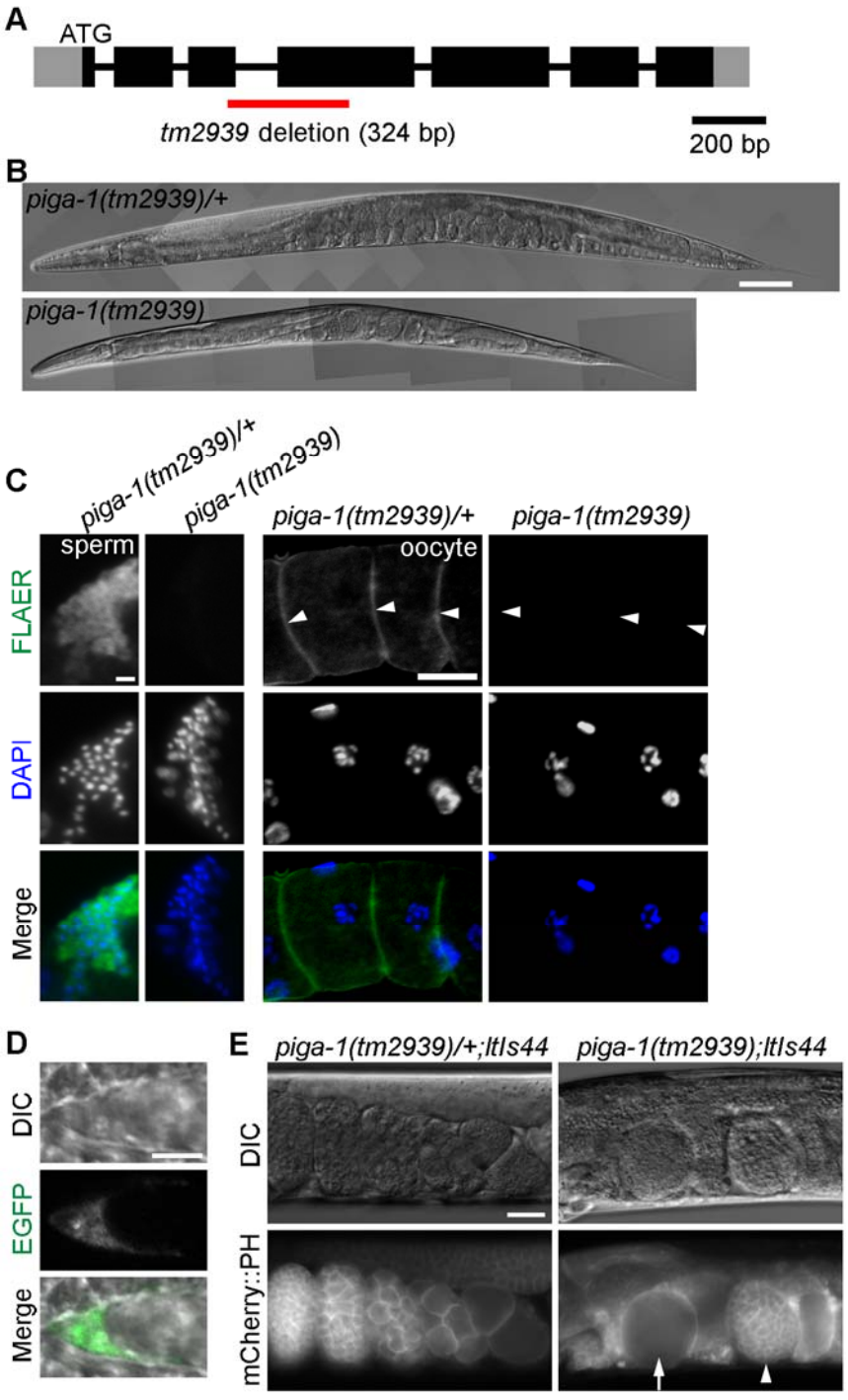
A
ATG
tm2939 deletion (324 bp)
200 bp
B
piga-1(tm2939)/+
piga-1(tm2939)
C
piga-1(tm2939)/+
piga-1(tm2939)
piga-1(tm2939)/+
piga-1(tm2939)
sperm
oocyte
FLAER
DAPI
Merge
D
DIC
EGFP
Merge
E
piga-1(tm2939)/+;ltIs44
piga-1(tm2939);ltIs44
DIC
mCherry::PH

Figure 6. Knockout of *piga-1* results in a germline-lethal phenotype.
(A) Structure of the *piga-1* gene. Black and gray boxes indicate exons and untranslated regions, respectively. The red line indicates the region deleted in the *tm2939* allele.
(B) Although *piga-1(tm2939)/+* worms showed no apparent phenotype, *piga-1(tm2939)* worms showed reduced body length and various abnormalities. Bar, 100 μm.
(C) GPI-anchored proteins were absent in *piga-1(tm2939)* homozygous worms. No FLAER staining was observed in dissected gonads of the *piga-1(tm2939)* worms, while bright staining was observed in gonads of the *piga-1(tm2939)/+* worms. Arrowheads indicate oocyte membranes. Bars, 5 μm (left column) and 20 μm (right column).
(D) The GPI-anchored protein WRK-1 was mislocalized in *piga-1* knockout worms. EGFP-tagged WRK-1 was not present on the surface of DTCs but instead remained inside the cells. Bar, 5 μm.
(E) Abundant abnormal eggs in the uteri of *piga-1(tm2939);ltIs44* worms. Non-dividing eggs (arrow) and dividing eggs at the multicellular stage (arrowhead) were present but all were nonviable. Bar, 20 μm.

Figure 7

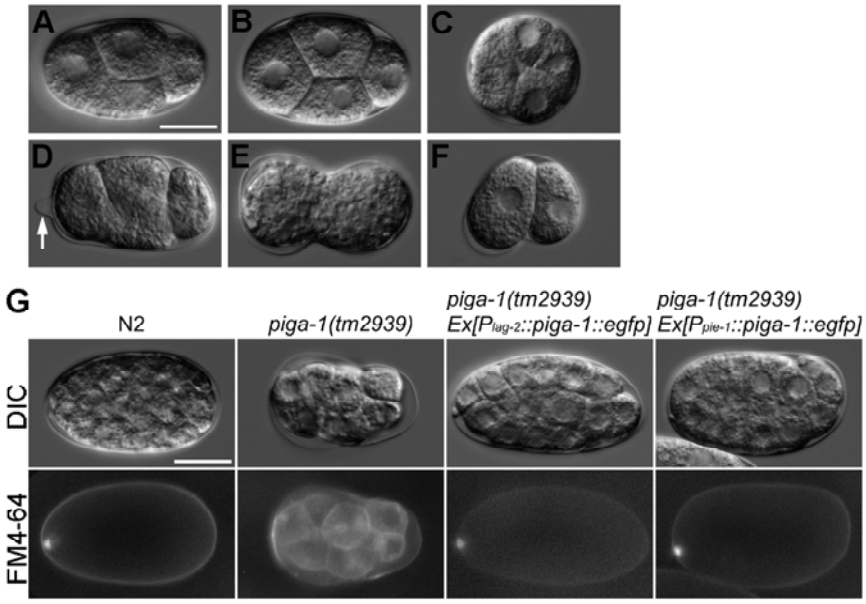

Figure 7. Abnormal egg morphology and eggshell permeability of the *piga-1(tm2939)* embryos.
(A) Wild-type embryo.
(B-F) *piga-1(tm2939)* embryos. (B) Apparently normal embryo. (C) Spherical embryo. (D) Embryo with protruding egg shell (arrow). (E) Embryo with constriction in the middle. (F) Embryo bent in the middle.
(G) Eggshell permeability of the wild-type and the *piga-1(tm2939)* embryos. The lipophilic dye FM4-64 stains cell membranes. In wild-type N2 and rescued *piga-1(tm2939)* embryos, only eggshells and polar bodies were stained. In the *piga-1(tm2939)* embryos, their eggshells were permeable to FM4-64, and the cell membranes of the embryos were stained.
Bars, 20 μm.

Figure 8

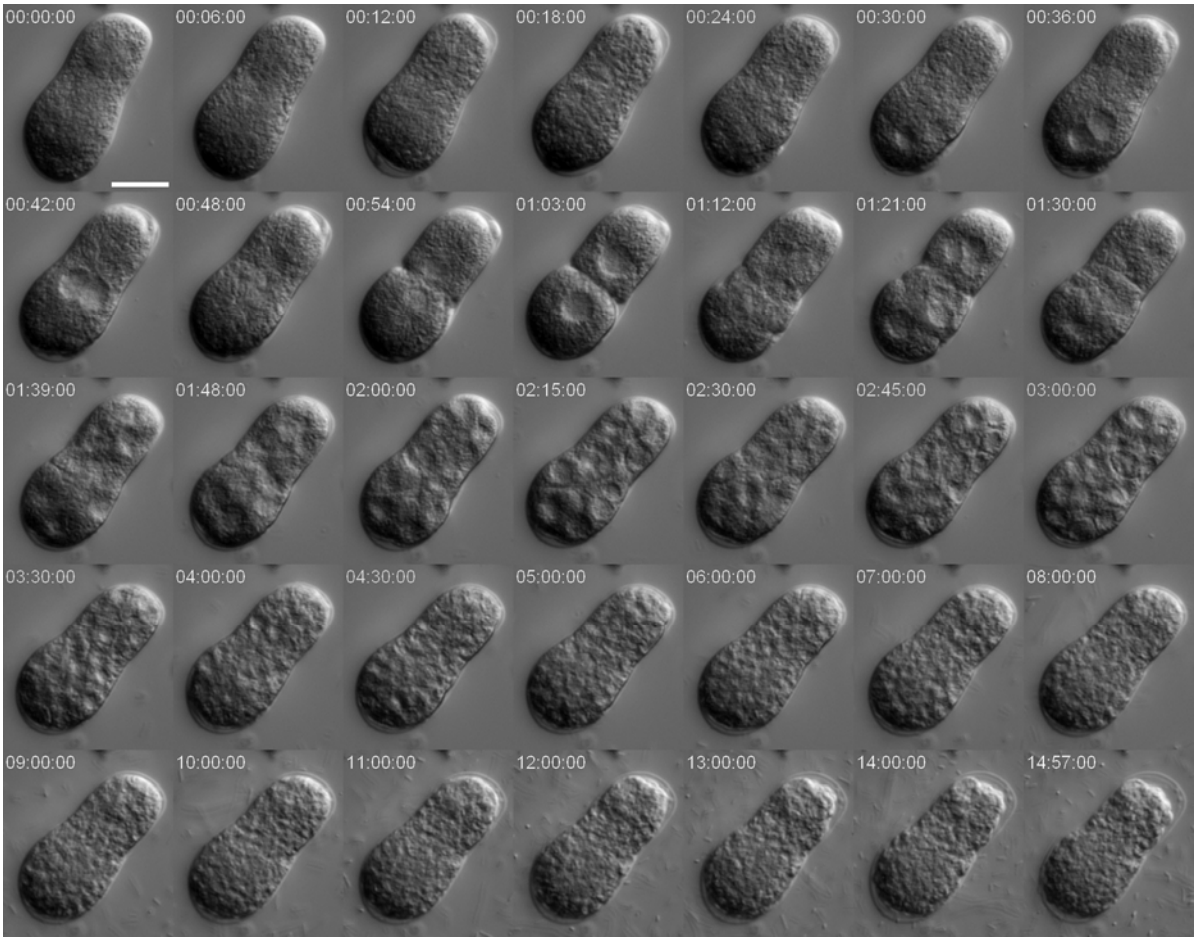

Figure 8. Abnormal embryonic cell division of the *piga-1(tm2939)* embryo under osmotic supported condition.
Note the abnormal shape of the eggshell, and the abnormal orientation of cell divisions. Bar, 20 μm. Digits at the top indicate the time passed in “h: min: sec” format.

Figure 9

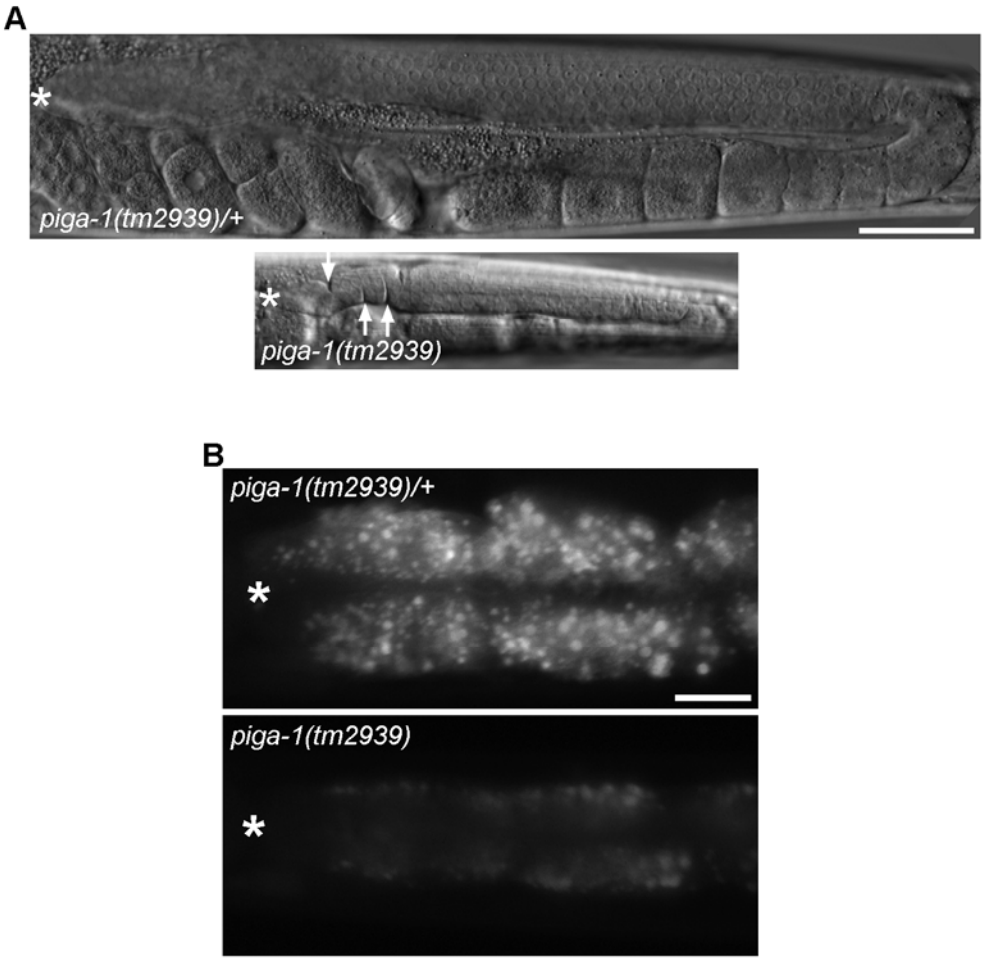

Figure 9. Abnormalities of somatic tissues in the *piga-1(tm2939)* worm.
(A) Gonads of *piga-1(tm2939)*/+ and *piga-1(tm2939)* worms. Gonad size was decreased in *piga-1(tm2939)* worms. Some animals showed wrinkled gonadal arms (arrows). Asterisks indicate DTCs.
(B) Intestines of *piga-1(tm2939)*/+ and *piga-1(tm2939)* worms. Autofluorescent granules in the intestinal cells were visualized using a DAPI filter under UV illumination. Autofluorescence of the granules was decreased in the intestine of *piga-1(tm2939)* worms. Asterisks indicate the position of the pharyngeal-intestinal valve.
Bars, 50 μm (A) and 20 μm (B).

Figure 10

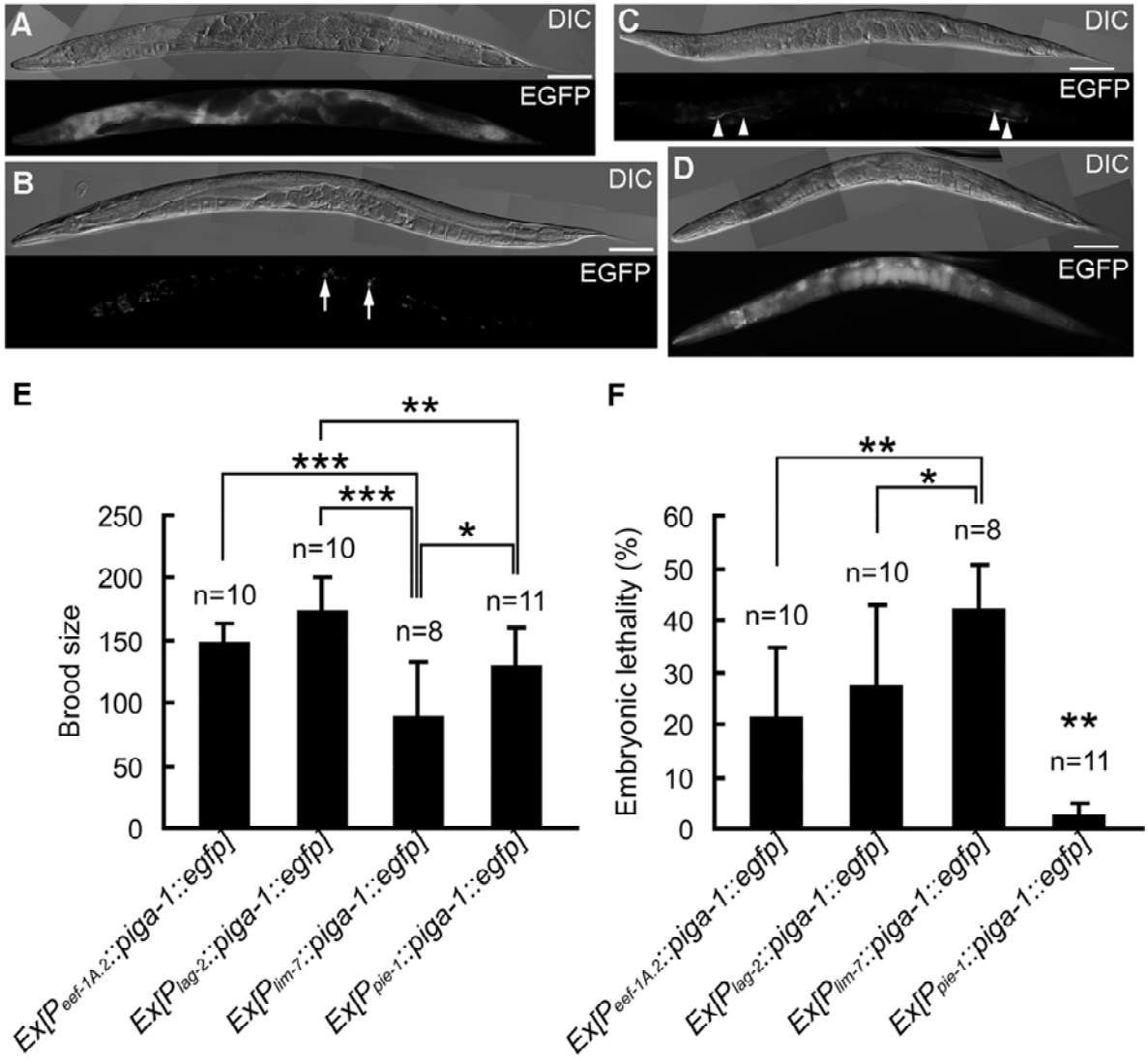

Figure 10. Tissue-specific rescue of the *piga-1(tm2939)* mutant.
(A-D) DIC and fluorescence images of the *piga-1(tm2939)* rescue lines 24 h after the L4 stage. (A) *piga-1(tm2939) Ex[$P_{eef-1A.2}$::piga-1::egfp, pRF4]*. EGFP expression was observed in all cells except for germline cells and early embryos. (B) *piga-1(tm2939) Ex[P_{lag-2}::piga-1::egfp, pRF4]*. EGFP expression was detected in DTCs (arrows). Nonspecific gut granule fluorescence was also observed in the intestine. (C) *piga-1(tm2939) Ex[P_{lim-7}::piga-1::egfp, pRF4]*. EGFP expression was observed in gonadal sheath cells (arrowheads). (D) *piga-1(tm2939) Ex[P_{pie-1}::piga-1::egfp, pRF4]*. EGFP expression was detected in embryos in utero. Autofluorescence was also observed in the pharynx and intestine. Bars, 100 μm.
(E and F) Brood size and embryonic lethality in the *piga-1(tm2939)* rescue lines. Brood size was reduced (E) and embryonic lethality was increased (F) in the *P_{lim-7}::piga-1::egfp* rescue line compared with the *$P_{eef-1A.2}$::piga-1::egfp*, *P_{lag-2}::piga-1::egfp*, and *P_{pie-1}::piga-1::egfp* rescue lines. The *P_{pie-1}::piga-1::egfp* transgene rescued the defects most effectively. Embryonic lethality is indicated by the percentage of unhatched eggs. The data for the most effectively rescued line are displayed. Bar graphs represent the mean values of brood size and embryonic lethality. Error bars indicate S.D. * indicates $P < 0.05$, ** indicates $P < 0.01$ and *** indicates $P < 0.001$ (Holm's multiple comparison test).

Figure 11

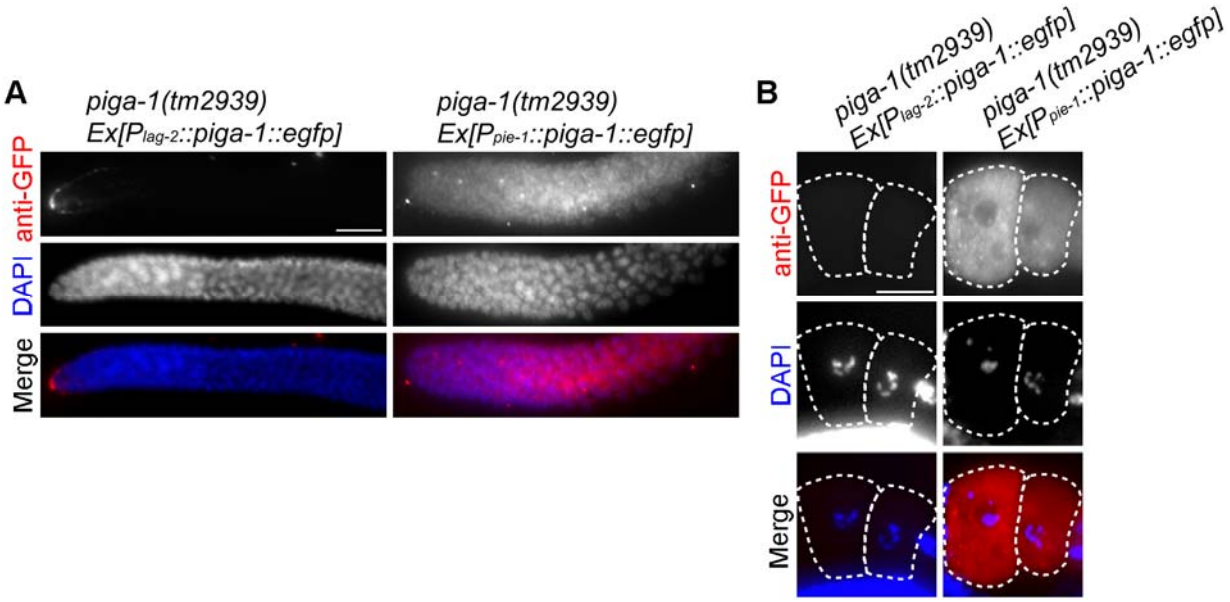

Figure 11. Immunofluorescent staining of the rescued *piga-1(tm2939)* worms using the anti-GFP antibody.
(A) In the distal gonad, the fluorescent signal was detected only in DTCs in *piga-1(tm2939) Ex[P_{lag-2}::piga-1::egfp*] (left column). The signal was observed all over the germline in *piga-1(tm2939) Ex[P_{pie-1}::piga-1::egfp*] (right column).
(B) In oocytes, the fluorescent signal was detected in *piga-1(tm2939) Ex[P_{pie-1}::piga-1::egfp*] but not in *piga-1(tm2939) Ex[P_{lag-2}::piga-1::egfp*]. Dotted lines indicate outlines of oocytes.
Bars, 20 μm.

Figure 12

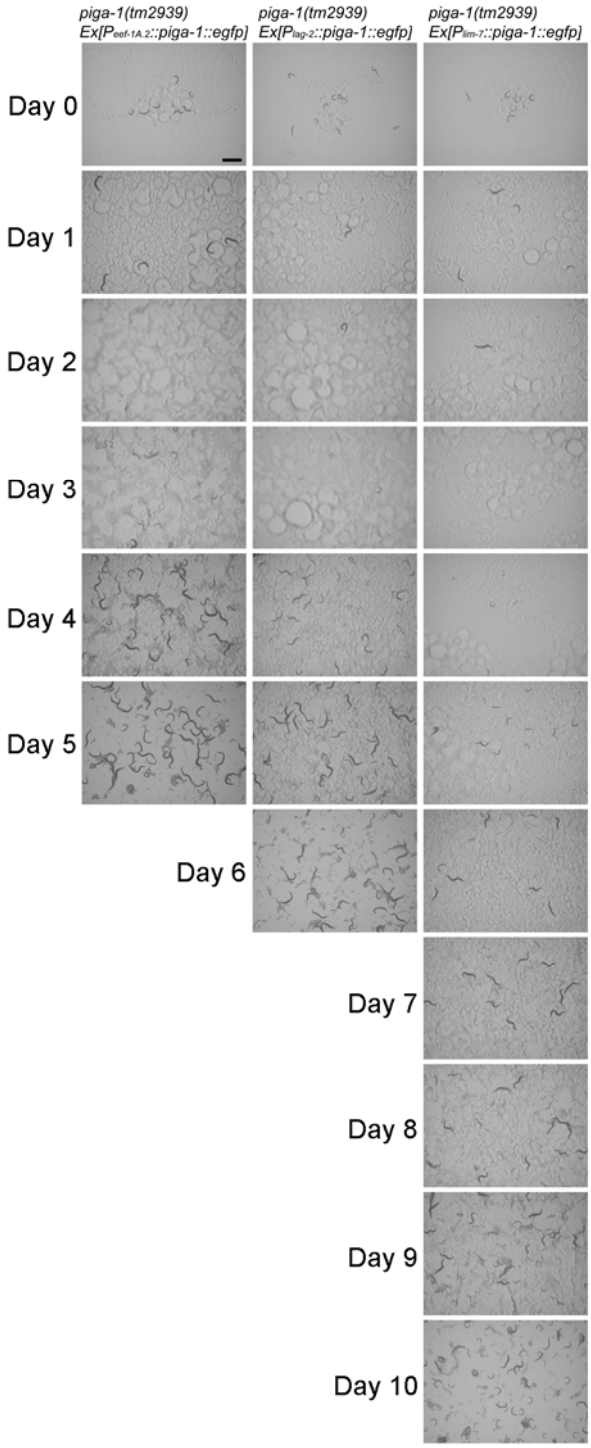

Figure 12. Growth of the *piga-1(tm2939)* rescue lines on NGM plate. Ten rescued L4 worms were placed on a fresh NGM plate seeded with OP50 and maintained at 20° C. Microscopic images of worms on the plates were acquired with an OLYMPUS SZX12 microscope (OLYMPUS) equipped with a digital camera (Nikon COOLPIX 990, Nikon) every 24 h until bacteria on the plate were depleted. The P_{lim-7}*::piga-1::egfp* rescue line showed slow growth and proliferation compared with the $P_{eef-1A.2}$*::piga-1::egfp* rescue line and the P_{lag-2}*::piga-1::egfp* rescue line. It took 10 days for the P_{lim-7}*::piga-1::egfp* rescue line to eat up all the OP50 bacteria on the plate, while it took 5 and 6 days for the $P_{eef-1A.2}$*::piga-1::egfp* rescue line and P_{lag-2}*::piga-1::egfp* rescue line, respectively. Bar, 1 mm (measured with an eyepiece micrometer).

Figure 13

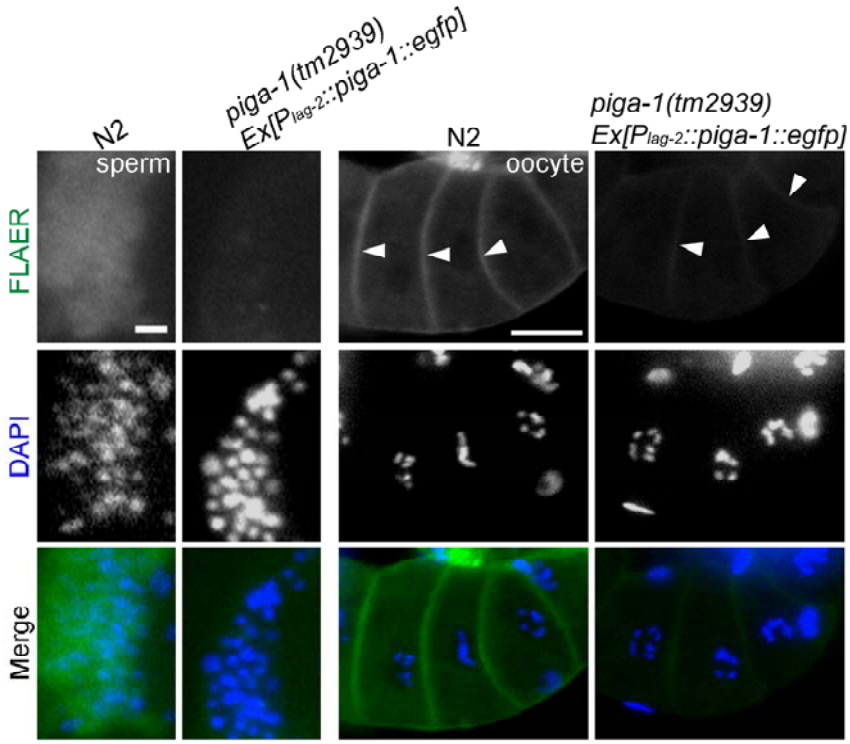

Figure 13. Weak FLAER staining was observed in the oocyte membrane of the rescued *piga-1(tm2939)* mutant compared with that of the wild-type animal.

No FLAER signal was detected in sperm of the rescued mutants. Arrowheads indicate oocyte membranes. Bars, 5 μm (left column) and 20 μm (right column).

Figure 14

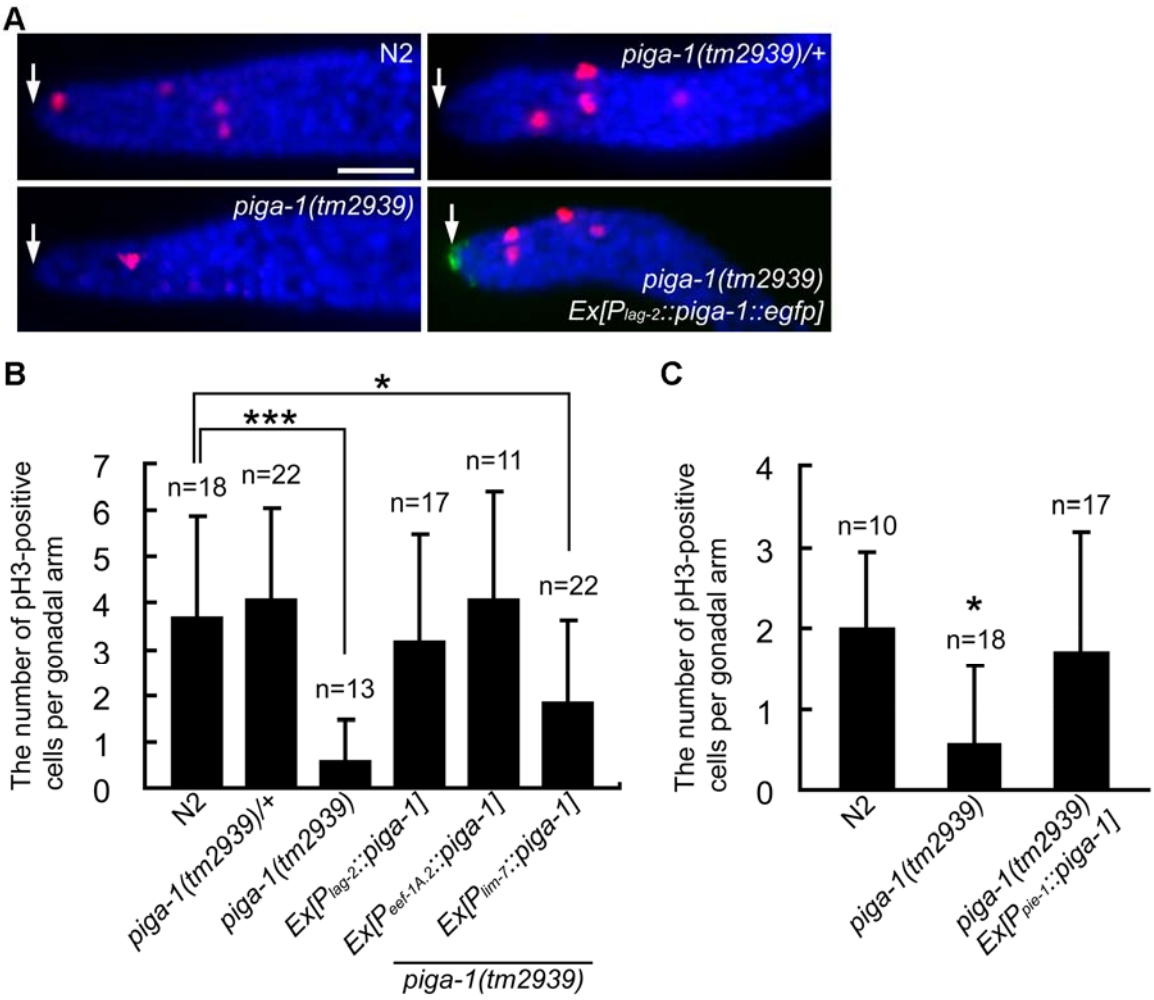

Figure 14. The number of mitotic germ cells at the distal gonad was decreased in *piga-1(tm2939)* worms.
Normal numbers of mitotic germ cells were detected in N2 and *piga-1(tm2939)/+* worms and in worms rescued with the transgene.
(A) Immunofluorescent staining using the anti-pH3 antibody. Red, cells stained with the anti-pH3 antibody; blue, DAPI-stained DNA; green, PIGA-1::EGFP. Arrows indicate DTCs. Bar, 20 μm.
(B and C) Bar graphs represent the mean numbers of pH3-positive cells at 20° C (B) and 25° C (C). Error bars indicate S.D. * indicates $P < 0.05$, and *** indicates $P < 0.001$ (Holm's multiple comparison test).

Figure 15

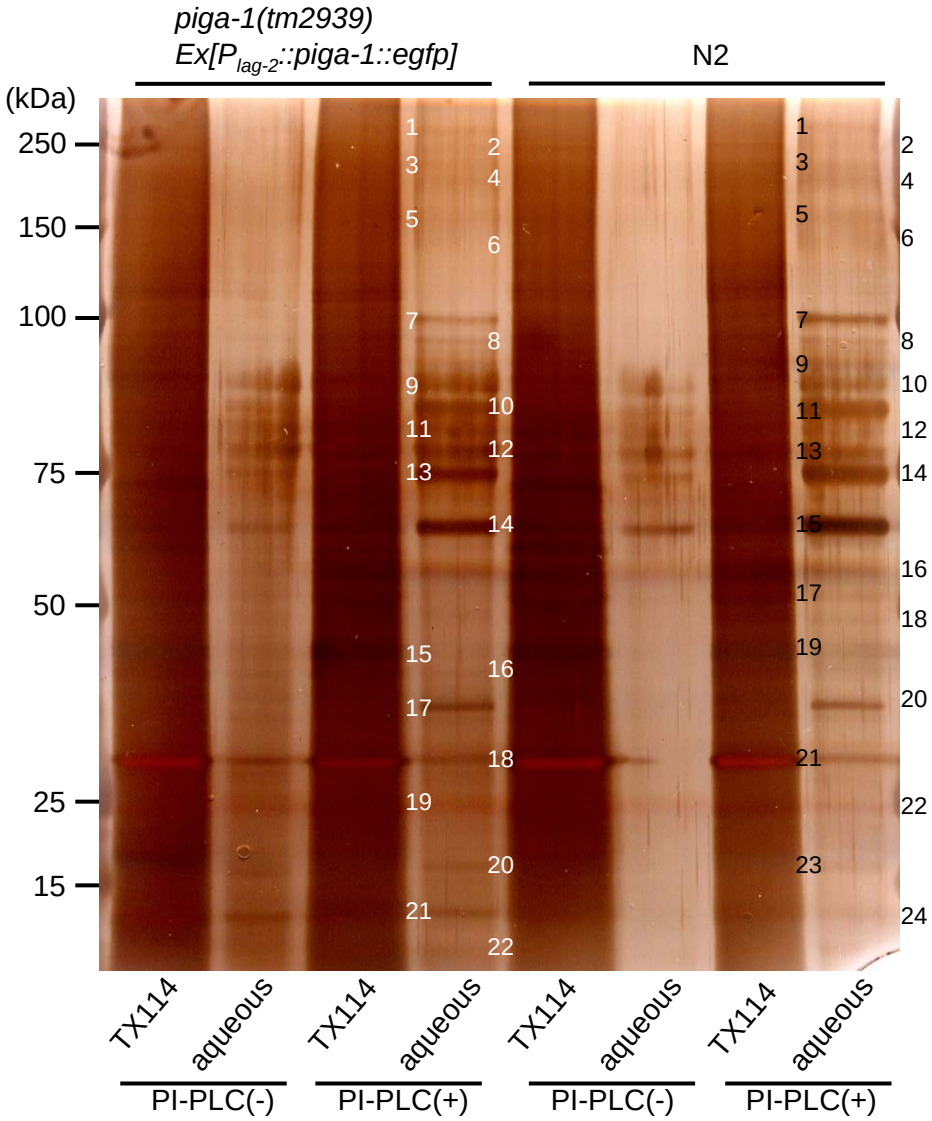

Figure 15. The extracted GPI-anchored proteins were separated by SDS-PAGE and stained with Silver stain MS kit (Wako).
The silver-stained gel including samples before PI-PLC treatment (PI-PLC (-)) and after PI-PLC treatment (PI-PLC(+)) is shown. Numbers indicate the positions of possible GPI-anchored protein bands. Black numbers, N2; white numbers, *piga-1(tm2939) Ex[P$_{lag-2}$::piga-1::egfp]*.

Table 1

Band	CDS/ Public name	Description	Phenotype	Human homolog
1	Y16B4A.2	serine-type carboxypeptidase activity	n/a	lysosomal protective proteine isoform a precursor
4	Y41D4B.16/ hpo-6	uncharacterized	n/a	isoform 2 of mucin-3A
6	F23B2.11/ pcp-3	prolyl carboxypeptidase like	n/a	thymus-specific serine protease
	Y40D12A.2	serine carboxypeptidases (lysosomal cathepsin A)	Lva, Emb, protein aggregation variant	lysosomal protective protein isoform a precursor
	C29F3.7	positive regulation of growth rate	maternal Ste	n/a
7	F32A5.3	serine carboxypeptidases (lysosomal cathepsin A)	n/a	lysosomal protective protein isoform a precursor
	C31C9.1/ tag-10	apical gut membrane polyprotein	n/a	n/a
	C34H4.3/ tag-244	uncharacterized	n/a	n/a
	F53C11.1	uncharacterized	n/a	n/a
	K08D8.6	uncharacterized	n/a	n/a
8	Y47H9C.1	uncharacterized	n/a	n/a
9	T03G6.3	type I phosphodiesterase/nucleotide pyrophosphatase	n/a	ENPP6
	C53B7.1/ rig-3	neuronal IGCAM	Ste, Let	isoform 5 of neural cell adhesion molecule 1
	F54E2.1	uncharacterized	brood size variant	n/a
	R173.1/ cah-5	carbonic anhydrase	n/a	carbonic anhydrase 7
	F41D9.3/ wrk-1	ephrin receptor-interacting immunoglobulin superfamily protein	n/a	MAM domain-containing GPI-anchored protein 2
10	F35E12.10	uncharacterized	n/a	n/a
	ZK6.10/ dod-19	determination of adult life span	ventral cord patterning variant	n/a
11	ZK6.11a	uncharacterized	ventral cord patterning variant	n/a
	C05D9.3	integrin beta subunit	maternal Ste	isoform β-3A of integrin β-3
	F13B6.1	determination of adult life span	Emb	n/a
12	Y119C1B.9	uncharacterized	n/a	n/a

Table 1. The list of possible GPI-anchored proteins identified in N2 by SyproRuby staining (Figure 1C).
Ste, sterile; Emb, embryonic lethal; Let, Lethal; Lva, Larval arrest

Table 2

Human gene	*C. elegans* ortholog	Identity (%)	RNAi phenotypes	Human gene	*C. elegans* ortholog	Identity (%)	RNAi phenotypes
PIGA	*piga-1 (D2085.6)*	52	WT	*PIGG*	*F28C6.4*	40	WT
PIGC	*T20D3.8*	32	WT	*PIGK*	*T05E11.6*	52	Stp† (15%, *n*=510)
PIGH	Not found	-	-	*PIGS*	*T14G10.7*	39	WT
PIGP	*Y48E1B.2*	45	Stp* (32%, *n*=576)	*PIGT*	*F17C11.7*	26	WT
PIGQ	*F01G4.5*	34	WT	*PIGU*	*T22C1.3*	26	Stp† (14%, *n*=542)
PIGY	Not found	-	-	*GAA1*	*F33D11.9*	25	Stp† (14%, *n*=614)
PIGL	Not found	-	-	*PGAP1*	*T19B10.8*	29	WT
PIGW	*Y110A2AL.12*	31	WT	*PGAP5*	*B0511.13*	35	WT
PIGM	*B0491.1*	42	WT	*PGAP3*	*R01B10.4*	31	WT
PIGX	*F49E7.2*	42	WT	*PGAP2*	*T04A8.12*	40	WT
PIGV	*T09B4.1*	24	Stp† (18%, *n*=562)	The following genes are also involved in N-/O-glycosylation.			
PIGN	*Y54E10BR.1*	34	WT	*DPM1*	*dpm-1 (Y66H1A.2)*	65	Sck (100%, *n*=408) Lva (92%, *n*=408)
PIGB	*T27F7.4*	36	WT	*DPM2*	Not found	-	-
PIGF	Not found	-	-	*DPM3*	*dpm-3 (F28D1.11)*	45	Emb (40%, *n*=698) Stp (10%, *n*=698)
PIGO	*C27A12.9*	41	Stp† (15%, *n*=519)	*MPDU1*	*F38E1.9*	40	Stp (13%, *n*=580)

Table 2. Genes involved in GPI-anchor synthesis in *C. elegans*.
Identities indicate the percentage of amino-acid-sequence identities. WT, wild-type; Stp, sterile progeny phenotype; Sck, Sick phenotype; Lva, larval arrest phenotype; Emb, embryonic lethal phenotype. * Sterility with the abnormal oocyte maturation (see Figure 3, A, C and D); † Sterility with the fertilization defect (see Figure 3E).

Table 3

Strain	Permeable eggshell (%)	*n*
N2	0	70
piga-1(tm2939)	25.4	67
piga-1(tm2939) *Ex[P$_{lag-2}$::piga-1::egfp]*	0	74
piga-1(tm2939) *Ex[P$_{pie-1}$::piga-1::egfp]*	0	70

Table 3. Eggshell permeability to the lipophilic dye FM4-64.

Table 4

Transgene	Expression tissue	Obtained transgenic lines	Rescue lines
$P_{eef\text{-}1A.2}$*::piga-1::egfp*	almost all cells	2	2
$P_{lag\text{-}2}$*::piga-1::egfp*	distal tip cells	8	8
$P_{lim\text{-}7}$*::piga-1::egfp*	gonadal sheath cells	7	5
$P_{pie\text{-}1}$*::piga-1::egfp*	germline and embryos	2	2
$P_{sth\text{-}1}$*::piga-1::egfp*	spermatheca and uterus	3	0
$P_{myo\text{-}3}$*::piga-1::egfp*	muscles	7	0
$P_{rgef\text{-}1}$*::piga-1::egfp*	pan-neurons	6	0

Table 4. Transgenic rescue experiments of *piga-1(tm2939)* mutants with wild-type *piga-1* genes driven by different promoters.

Table 5

Band	CDS/ Public name	Description	Phenotype	Human homolog
1	F57F4.4	positive regulation of growth rate	Ste, Emb, Sck, Let	stabilin-2
	F57F4.3*/ gfi-1	positive regulation of growth rate	locomotion variant	mucin-5AC (fragment)
6	Y41D4B.16*/ hpo-6	uncharacterized	n/a	isoform 2 of mucin-3A
	F23B2.11*/ pcp-3	prolyl carboxypeptidase like	n/a	thymus-specific serine protease
9	K11H12.4*	uncharacterized	n/a	n/a
	ZK896.5	uncharacterized	n/a	n/a
9	F19C7.2	serine-type peptidase activity	n/a	thymus-specific serine protease
10	C31C9.1a*/ tag-10	apical gut membrane polyprotein	n/a	n/a
	K08D8.6*	uncharacterized	n/a	n/a
	F56F10.1	serine-type peptidase activity	n/a	thymus-specific serine protease
11	C34H4.3*/ tag-244	uncharacterized	n/a	n/a
	T16D1.2/ pho-4	acid phosphatase activity	n/a	lysosomal acid phosphatase
	T03G6.3*	type I phosphodiesterase/nucleotide pyrophosphatase	n/a	ENPP6
	W05E10.4a*/ tre-3	alpha,alpha-trehalase activity	n/a	isoform 1 of trehalase
	W05E10.4b*/ tre-3	alpha,alpha-trehalase activity	n/a	isoform 1 of trehalase
12	F54E2.1*	uncharacterized	brood size variant	n/a
	C34B7.1	a divergent MYST acetyltransferase	n/a	n/a
13	C34H4.1*	integral to membrane	n/a	n/a
	C05D9.3*	integrin beta subunit	maternal Ste	isoform b-3A of integrin b-3
	F44E2.4	predicted receptor-like serine/threonine kinase	protein aggregation variant	low density lipoprotein receptor
14	ZK6.10*/ dod-19	determination of adult life span	ventral cord patterning variant	n/a
	F35E12.10*	uncharacterized	n/a	n/a
16	F44D12.2	transmembrane receptor protein S/T kinase activity	n/a	n/a
17	ZK6.11a*	uncharacterized	ventral cord patterning variant	n/a
18	F15G9.5	uncharacterized	n/a	n/a
	F01G10.6	uncharacterized	n/a	n/a
	F32A5.3	serine carboxypeptidases (lysosomal cathepsin A)	n/a	lysosomal protective protein isoform a precursor
19	F54E4.3*	uncharacterized	n/a	n/a
	R173.1 */ cah-5	carbonic anhydrase	n/a	carbonic anhydrase 7
20	C44B7.5*	dopamine beta-monooxygenase activity	n/a	n/a
	F27E5.4*/ phg-1	embryonic development ending in birth or egg hatching, mitosis	Slo, mitosis variant	growth arrest-specific protein 1
21	D1054.10	uncharacterized	n/a	n/a
22	K12B6.9	uncharacterized	n/a	n/a
23	K11H12.7	uncharacterized	n/a	n/a
	Y40D12A.2*	serine carboxypeptidases (lysosomal cathepsin A)	Lva, Emb, protein aggregation variant	lysosomal protective protein isoform a precursor
24	C15H9.9*	uncharacterized	n/a	n/a

Table 5. The list of possible GPI-anchored proteins identified in N2 by silver staining (Figure 15).
Ste, sterile; Emb, embryonic lethal; Let, Lethal; Sck, unhealthy; Slo, Slow growth rate; Lva, Larval arrest. Proteins listed both in Table 5 and 6 are indicated with asterisks.

Table 6

Band	CDS/ Public name	Descripttion	Phenotype	Human homolog
2	F15E11.4	predicted receptor	n/a	n/a
	C12D12.1a	uncharacterized	n/a	mucin-2
3	F57F4.3* gfi-1	positive regulation of growth rate	locomotion variant	mucin-5AC (fragment)
	Y16B4A.2	serine-type carboxypeptidase activity	n/a	lysosomal protective proteine isoform a precursor
6	Y41D4B.16*	uncharacterized	n/a	isoform 2 of mucin-3A
7	W05E10.4a*/ tre-3	alpha,alpha-trehalase activity	n/a	isoform 1 of trehalase
	W05E10.4b*/ tre-3	alpha,alpha-trehalase activity	n/a	isoform 1 of trehalase
8	Y37E11AR.6/ vab-2	ephrin, ligand for ephrin receptor tyrosine kinase	head notched, head morphology variant, aldicarb hypersensitive, oraganism morphology variant	ephrin-B2
	F35E12.8a	uncharacterized	n/a	n/a
	F23B2.11*/ pcp-3	prolyl carboxypeptidase like	n/a	thymus-specific serine protease
9	ZK896.4	uncharacterized	n/a	n/a
	C31C9.1a* / tag-10	apical gut membrane polyprotein	n/a	n/a
	K08D8.6*	uncharacterized	n/a	n/a
	F58H7.1	uncharacterized	n/a	collagen, type XI, α 2
10	T03G6.3*	type I phosphodiesterase/nucleotide pyrophosphatase	n/a	ENPP6
	F54E2.1*	uncharacterized	brood size variant	n/a
	C34H4.3*/ tag-244	uncharacterized	n/a	n/a
11	K11H12.4*	uncharacterized	n/a	n/a
12	C05D9.3*	integrin beta subunit	maternal Ste	isoform β-3A of integrin β-3
	C34H4.1*	unnamed protein	n/a	n/a
	F35E12.10*	uncharacterized	n/a	n/a
13	ZK6.10*/ dod-19	determination of adult life span	ventral cord patterning variant	n/a
14	ZK6.11a*	uncharacterized	ventral cord patterning variant	n/a
16	R173.1*/ cah-5	carbonic anhydrase	n/a	carbonic anhydrase 7
	Y40D12A.2*	serine carboxypeptidases (lysosomal cathepsin A)	Lva, Emb, protein aggregation variant	lysosomal protective protein isoform a precursor
17	C44B7.5*	dopamine beta-monooxygenase activity	n/a	n/a
19	F54E4.3*	uncharacterized	n/a	n/a
21	C15H9.9*	uncharacterized	n/a	n/a
	F27E5.4*/ phg-1	embryonic development ending in birth or egg hatching, mitosis	Slo, mitosis variant	growth arrest-specific protein 1
22	C02B10.3	a predicted secreted protein containing EGF-like repeats	n/a	cDNA FLJ51576, highly similar to Jagged-1

Table 6. The list of possible GPI-anchored proteins identified in *piga-1(tm2939) Ex[P_{lag-2}::piga-1::egfp]* by silver staining (Figure 15).
Ste, sterile; Emb, embryonic lethal; Slo, Slow growth rate; Lva, Larval arrest. Proteins listed both in Table 5 and 6 are indicated with asterisks.

Table 7

Amplified products		Primer sequences
Y48E1B.2 cDNA	Forward	5'- AAACTCCAAAAACCCCACTACC -3'
	Reverse	5'- TTCCTGTCGTTCCTTCTTCC -3'
T27F7.4 cDNA	Forward	5'- ATGCGCACTACACTTCGTTT -3'
	Reverse	5'- GTACCCATTCCGACACAACAC -3'
C27A12.9 cDNA	Forward	5'- ATGGGATCAATAATTCGAATACTC -3'
	Reverse	5'- GCTTCACTATTCTTGAATTTCTCG -3'
T22C1.3 cDNA	Forward	5'- ATGGCAAAGGACAAGAAATTACA -3'
	Reverse	5'- GTCGTCGCGAGTAAACGAAG -3'
B0511.13 cDNA	Forward	5'- ATGATATGGCTTAAAAATTTGCGA -3'
	Reverse	5'- CTGTTCAGAGCCGGTTGATT -3'
dpm-1 genomic sequence	Forward	5'- TTTCAGATTATTATGACATCCACTCC -3'
	Reverse	5'- CCAAACAAATGCAAACAGATAGA -3'
lag-2 promoter	Forward	5'- CCGGAATTTTGATTGTAGGC -3'
	Reverse	5'- CATTTTCTGAAAAAAGGCAAAT -3'
lim-7 promoter	Forward	5'- GAGGTTGGCTGATCCCTCTC -3'
	Reverse	5'- TTCTGAAAAATGAAAGCTCGATTAAC -3'
sth-1 promoter	Forward	5'- TCTCCCTGATCTGGATTGGA -3'
	Reverse	5'- CATGTTGCTCTAGCACAAAAAGAC -3'
pie-1 promoter	Forward	5'- AATTGAAAGTTTTGTGGGGAAA -3'
	Reverse	5'- CTGGAAAAGAAAATTTGATTTTTAAT -3'
pie-1 3rd intron	Forward	5'- TAGGATCCGTGCTGATCGGATGGAAATT -3'
	Reverse	5'- TAGGATCCGGTCTCCGATTCTGGAAGTAAA -3'
pie-1 3' sequence	Forward	5'- TAAGATCTTTTTGCCGTATTTTCCATATTTT -3'
	Reverse	5'- TAACATGTCAGGATTTTTCCATCATTTTTCC -3'
piga-1 genomic sequence	Forward	5'- CACGCGGCCGCATGTCGCTAAAAATTGGTCCG -3'
	Reverse	5'- TATGCGGCCGCACTGATAGTCAGGATCAACATTTTTC -3'
wrk-1 genomic sequence	Forward	5'- TATGCGGCCGCATGATGAAATTGGTTCTGCT -3'
	Reverse	5'- TATAGATCTTTAAAATAAAAGATACATTGTGACT -3'
wrk-1 promoter	Forward	5'- TATGCGGCCGCCTCTTTCTCGATGCCCTTCT -3'
	Reverse	5'- TATGCGGCCGCCTGAAAAAAGAAAATGTTGAAAA -3'
egfp	Forward	5'- TATGGATCCATGGTGAGCAAGGGCGAG -3'
	Reverse	5'- TATGGATCCCTTGTACAGCTCGTCCATGC -3'

Table 7. The list of primers used in plasmid construction.
Restriction sites are underlined.